Hygroscopicity of organic surrogate compounds from biomass burning and their effect on the efflorescence of ammonium sulfate in mixed aerosol particles

Ting Lei[1,2], Andreas Zuend[4], Yafang Cheng[2,3], Hang Su[2,3], Weigang Wang[1], Maofa Ge[1*]

[1]State Key Laboratory for Structural Chemistry of Unstable and Stable Species, CAS Research/Education Center for Excellence in Molecular Sciences, Institute of Chemistry, Chinese Academy of Sciences, Beijing, 100190, P. R. China

[2]Multiphase Department, Max Planck Institute for Chemistry, Mainz 55128, Germany

[3]Institute for Environmental and Climate Research, Jinan University, Guangzhou, China

[4]Department of Atmospheric and Oceanic Sciences, McGill University, Montreal, Quebec, Canada

Correspondence to: M. F. Ge (gemaofa@iccas.ac.cn)

Abstract: Hygroscopic growth factors of organic surrogate compounds representing biomass burning and mixed organic-inorganic aerosol particles exhibit variability during dehydration experiments depending on their chemical composition, which we observed using a hygroscopicity tandem differential mobility analyzer (HTDMA). We observed that levoglucosan and humic acid aerosol particles release water upon dehumidification in the range from 90 – 5 % relative humidity (RH). 4-Hydroxybenzoic acid aerosol particles, however, remain in the solid state both upon dehumidification or dehumidification and exhibit a small shrinking in size at higher RH compared to the dry size. For example, the measured growth factor of 4-hyroxybenzoic acid aerosol particles is ~0.96 at 90 % RH. The measurements were accompanied by RH-dependent thermodynamic equilibrium calculations using the AIOMFAC and the E-AIM models, the ZSR relation, and a fitted hygroscopicity expression. We observed several effects of organic components on the hygroscopicity behavior of mixtures containing ammonium sulfate (AS) in relation to the different mass fractions of organic compounds: (1) a shift of efflorescence relative humidity (ERH) of ammonium sulfate to higher RH due to the presence of 25 wt % levoglucosan in the mixture. (2) There is a distinct efflorescence transition at 25 % RH for mixtures consisting of 25 wt % of 4-hydroxybenzoic acid compared to the ERH at 35 % for organic-free AS particles. (3) There is indication for a liquid-to-solid phase transition of 4-hydroxybenzoic acid in the mixed particles during dehydration.

29   (4) A humic acid component shows no significant effect on the efflorescence of AS in mixed aerosol

30   particles. In addition, consideration of a composition-dependent degree of dissolution of crystallization

31   AS (solid-liquid equilibrium) in the AIOMFAC and E-AIM models leads to a relatively good agreement

32   between models and observed growth factors, as well as ERH of AS in the mixed system. The use of the

33   ZSR relation leads to good agreement with measured diameter growth factors of aerosol particles

34   containing humic acid and ammonium sulfate. Lastly, two distinct mixtures of organic surrogate

35   compounds, including levoglucosan, 4-hydroxybenzoic acid, and humic acid were used to represent the

36   average water-soluble organic carbon (WSOC) fractions observed during the wet and dry seasons in the

37   central Amazon Basin. A comparison of the organic fraction's hygroscopicity parameter for the simple

38   mixtures, e.g. $\kappa \approx 0.12$ to 0.15 for the wet-season mixture in the 90 % to 40 % RH range, shows good

39   agreement with field data for the wet season in Amazon (WSOC $\kappa \approx 0.14\pm0.06$ at 90 % RH). This

40   suggests that laboratory-generated mixtures containing organic surrogate compounds and ammonium

41   sulfate can be used to mimic, in a simplified manner, the chemical composition of ambient aerosols from

42   the Amazon for the purpose of RH-dependent hygroscopicity studies.

43   **Introduction**

44   It is well established that biomass burning, as an important source of atmospheric aerosol particles, has

45   a wide range of climate effects that can be classified into direct radiative effects through light-absorbing

46   carbon aerosol particles and indirect effects by impact on cloud condensation nuclei and cloud

47   microphysics (Andreae and Gelencsér, 2006; Moosmüller et al., 2009; Hecobian et al., 2010; Rizzo et

48   al., 2011; Rose et al., 2011; Cheng et al., 2012; Engelhart et al., 2012; Lack et al., 2012; Jacobson, 2014;

49   Liu et al., 2014; Saleh et al., 2013, 2014). Atmospheric light-absorbing particles that arise from biomass

50   burning play an important role as a driver of global warming (Favez et al., 2009; Hegg et al., 2010; Lack

51   et al., 2012; Feng et al., 2013; Laborde et al., 2013; Srinivas and Sarin, 2013). According to the IPCC

52   report (Boucher and David, 2013), the climate forcing of black carbon aerosol particles may rival that of

53   methane, with a present-day global warming effect of up to 0.3–0.4 °C (Wang et al., 2014). Also, certain

54   types of aerosol particles emitted by biomass burning, when immersed into cloud droplets, absorb solar

55   radiation and facilitate water evaporation and cloud dispersion, which indicates an additional indirect

56   aerosol effect that counteracts the cooling effect of cloud droplets nucleated by aerosols (Powelson et al.,

57   2014). Therefore, a better understanding of the influence of aerosol particles from biomass burning on

58 cloud formation, precipitation, and Earth's radiative budget is required to comprehend biomass burning

59 aerosol properties and behavior.

60   The understanding of aerosol-cloud-climate impact of a vast range of biomass burning derived organic

61 compounds, however, is rather limited due to the complexity of biomass burning emissions, gas- and

62 aerosol-phase processing and the restricted availability of field measurements (Pratt et al., 2011; Lei et

63 al., 2014; Paglione et al., 2014; Srinivas and Sarin, 2014; Zhong and Jang, 2014; Ciarelli et al., 2015;

64 Arnold et al., 2015; Lawson et al., 2015; Gilman et al., 2015). Moreover, biomass burning particles are

65 often mixtures of water-soluble organic carbon, black carbon, varying amounts of inorganic components,

66 and water insoluble inclusions, such as mineral dust or poorly soluble organics (Väkevä et al., 2002;

67 Sadezky et al., 2005; Saarnio et al., 2010). An appreciable amount of organic compounds affect the

68 physicochemical properties of aerosols, such as hygroscopicity, liquid-solid and liquid-liquid phase

69 transitions, and chemical reactivity in liquid phases and/or on particle surfaces (Shiraiwa et al., 2013).

70 For example, equilibrium between the variable environmental water vapor mixing ratio and aerosol

71 particles may lead to substantial changes in particle size, and chemical composition, all of which can

72 influence light absorption and scattering (Seinfeld and Pandis, 2006; Zhang et al., 2016). RH-dependent

73 transitions between solid and liquid (aqueous) phases are also important in determining optical properties

74 (Martin et al., 2013; Wang et al., 2010; Kim et al., 2016; Wu et al., Denjean et al., 2015; 2016; Hodas et

75 al., 2015; Atkinson et al., 2015). Studies have shown that water-soluble organic matter from biomass

76 burning (approximately 70 % of total organic matter) can significantly suppress, enhance or have no

77 effect on the deliquescence (e.g. the RH at which deliquescence occurs at a certain temperature, the DRH)

78 and efflorescence process (e.g. the efflorescence RH, ERH) of present inorganic electrolytes. The effect

79 depends predominantly on the type of organics, mass fraction of organics relative to inorganic, and

80 particle size (You and Bertram, 2014; Zawadowicz et al., 2015; Hodas et al., 2015; Gupta et al., 2015).

81 Whole particles, individual phases within particles, or specific chemical compounds can undergo a range

82 of phase transitions including crystallization/efflorescence, dissolution/deliquescence, and liquid-liquid

83 phase separation as the relative humidity varies in the atmosphere. A number of laboratory studies have

84 focused on liquid-liquid phase separations within particles consisting of inorganic and organics fractions

85 (Svenningsson et al., 2006; Carrico et al., 2008; Dusek et al., 2011; Hodas et al., 2015). For example,

86 studies about liquid-liquid separation occurring in mixed organic-inorganic aerosols were performed by

87   Song et al. (2012, 2013) and You et al. (2013) using Raman and optical microscopy, establishing that

88   liquid-liquid phase separation occurs typically in mixed organics + ammonium sulfate particles with an

89   average elemental oxygen-to-carbon (O:C) ratio of the organic fraction of less than 0.6 and in some cases

90   for 0.6 < O:C < 0.8. You et al. (2013) further found that for a O:C ratio between 0.5 and 0.8, the

91   occurrence of liquid-liquid phase separation at moderate to high RH depends on the types of inorganic

92   salts present (i.e., the effective strength of the salting-out effect), e.g., $(NH_4)_2SO_4 \geq NH_4HSO_4 \geq NaCl \geq$

93   NH_4NO_3. Recently, the effect of a potential size-dependent morphology and dependence of the phase

94   separation mechanism on the organic/inorganic mass ratio in mixed aerosol was studied for mixtures of

95   poly- (ethylene glycol)-400 + ammonium sulfate using cryogenic-transmission electron microscopy

96   (Altaf et al., 2016). Therefore, many independent studies suggest that the occurrence of solid-liquid

97   and/or liquid-liquid phase separations, as well as related (temperature-dependent) RH levels of phase

98   transitions   (DRH, ERH, SRH), depend on the relative amounts of organic and inorganic aerosols

99   components and their non-ideal mixing behavior.

100   The expected physical state and morphology of aerosol particles containing mixtures of a wide range

101   of organic and inorganic salts/acids can, in principle, be predicted by a selection of specialized

102   thermodynamic equilibrium models. Such models include the Extended Aerosol Inorganic Model (E-

103   AIM) (Clegg and Seinfeld, 1998, 2006; available online: http://www.aim.env.uea.ac.uk/aim/aim.php),

104   the Aerosol Diameter Dependent Equilibrium Model (ADDEM) (Topping et al., 2004), the UNIversal

105   Quasichemical Functional Group Activity Coefficients model (UNIFAC) (Fredenslund et al.,1975;

106   Hansen et al., 1991), and the Aerosol Inorganic-Organic Mixtures Functional croups Activity

107   Coefficients model (AIOMFAC) (Zuend et al., 2008, 2011, 2012). These models have all been used to

108   predict atmospheric aerosol thermodynamic equilibrium for a variety of inorganic and organic systems,

109   yet not all of them can be used to compute non-ideal mixing in organic-inorganic systems. AIOMFAC

110   has been used to predict the distribution of components in multiple phases in a range of mixed organic-

111   inorganic systems and demonstrated its broad applicability in predicting liquid-liquid phase separation

112   in such mixtures (Zuend et al., 2010; Song et al., 2012; Zuend and Seinfeld, 2012; Shiraiwa et al., 2013;

113   Renbaum-Woff et al., 2016; Rastak et al., 2017).

114   Several previous experimental studies using the HTDMA technique (e.g. Zardini et al., 2008; Lei et

115   al.2014) show that the deliquescence of inorganic compounds is affected by the presence of organic

116 components, which manifests itself in a shift in the DRH of a salt compared to the corresponding organic-

117 free system. For instance, a clear shift of ammonium sulfate DRH was observed in the case of the

118 levoglucosan + ammonium sulfate system (Lei et al., 2014). Here we focus on investigating the

119 morphology, hygroscopicity and phase transitions of relevant organic compounds found in biomass

120 burning aerosol during the dehydration/dehumidification process. Moreover, we study how the presence

121 of organic compounds affects the water loss behavior of mixed organic-inorganic aerosols with

122 ammonium sulfate (AS) in the supersaturated state as well as after efflorescence of AS. In addition, we

123 compare the measured hygroscopicity behavior of mixed aerosol particles with predictions from the

124 Zdanovskii–Stokes–Robinson (ZSR) mixing rule, the E-AIM model and the AIOMFAC model.

125

126 **2 Methods**

127 **2.1 Aerosol system**

128 The three organic compounds levoglucosan, 4-hydroxybenzoic acid and humic acid were used as

129 surrogates for the rich-class of water-soluble organic components in biomass burning aerosols. The

130 influence of the distinct chemical structure of these compounds was studied with regard to the water

131 uptake and evaporation of the pure organic compounds as well as for mixed organic-AS-containing

132 particles. Furthermore, a comparison with field data from the Amazon was preformed to quantify the

133 ability of mixtures of these three organic compounds to mimicking the hygroscopic behavior of complex

134 ambient organic particles originating from biomass burning emissions. Here we focus on the

135 characterization of hygroscopic growth factors as well as solid-liquid and liquid-liquid phase transitions

136 during the dehumidification conditions. The chemical substances and their physical properties are

137 characterized in Table 1. All of the experimental solutions were prepared by dissolving in Milli-Q water

138 (resistivity $\geq$ 18.2 MΩ) and the experiments were conducted at room temperature (~298 K). For the

139 mixtures of ammonium sulfate and organic surrogates the different mass ratios of AS: organic considered

140 are 3:1, 1:1 1:3. The chemical compositions of biomass-burning model mixtures are introduced in Table

141 2.

142 **2.2 Instrument design**

143   Figure 1 shows a schematic of the HTDMA instrument, more detailed information about this instrument's

144   setup, calibration and evaluation is described elsewhere (Lei et al., 2014; Jing et al., 2015, 2017; Liu et

145   al., 2015). Briefly, Poly-dispersed sub-micrometer aerosol particles are generated by atomizing (MSP

146   1500, MSP) a 0.05 weight % aqueous solution consisting of different mass fractions of inorganic, and

147   organic components, assuming that the composition of the formed aerosol particles is initially the same

148   as that of the solution used in the atomizer. Aerosol particles from an atomizer are routed though

149   homemade silica diffusion dryers and then pass through a Nafion gas dryer (Perma Pure Inc., USA).

150   After aerosol particles were dried to below 5 % RH (RH set point 1, RH1), they are directed to the

151   impactor; those aerosols with diameter less than 1 μm are allowed to pass it and subsequently pass

152   through a ^{85}Kr electric charger to reach a near-Boltzmann distribution of charges (Liu et al., 1985). After

153   charging, the aerosol particles enter the first differential mobility analyzer (DMA1) at a sheath flow to

154   aerosol flow ratio of 4:0.3. The sheath flow is circulated by the diaphragm pump in the first loop DMA1

155   system, and its RH is kept constant at below 5 % RH. The resulting mono-disperse particle population,

156   selected within uncertainty by the DMA1, is then exposed to high RH conditions during which the aerosol

157   flow is humidified to 98 % RH by mixing water through a Nafion membrane humidifier at 30 °C. After

158   passing through a saturator (Perma Pure Inc., USA), the aerosols are dried to a target RH level (RH2)

159   through a series of two single-Nafion tubes (Perma Pure Inc., USA) with RH2 set to a value in the range

160   of 90 % to 5 % RH. Here, a pulse width modulator (PWM) circuit is used to regulate the sheath flow on

161   the basis of a proportional integral derivative (PID) system. When the second Nafion membranes allow

162   for regulating the sheath flow to a desired RH and for controlled flow into the sample stream until the

163   RH2 setting value is equal to the excess RH of sheath flow value (RH3), the mobility diameter of the

164   dehumidified of aerosols at target RH are measured with the second DMA (DMA2, a scanning DMA)

165   coupled with a condensation particle counter CPC (Model 1500, MSP). In addition, the residence time

166   between the humidifier and DMA2 is around 5 s, which is estimated to be sufficient for aerosols to grow

167   /shrink to equilibrium size at a certain RH setpoint. Also, due to recirculation of the sheath flow and the

168   pre-humidification of the aerosol flow, the sheath flow and aerosol sample flow are enabled to rapidly

169   reach the same RH.

170   **2.3 Theory and modeling methods**

171   Models were applied to explore the extent to which measured hygroscopic diameter growth factors

172 (HGFs), particle phase states, and phase compositions under sub-saturation conditions can be predicted

173 by thermodynamic equilibrium models. For the AS-containing systems studies, the current

174 thermodynamic equilibrium predictions account for a crystalline AS phase with solid-liquid equilibria

175 prior to the complete deliquescence of AS under hydration conditions. Similarly, the crystallization point

176 followed by a solid-liquid equilibrium of AS needs to be considered to predict the effect of organic

177 components in the mixed particles on the shift/suppression of AS efflorescence during aerosol

178 dehumidification, i.e. referring to processes occurring along the dehydration branch of a HTDMA

179 humidification-dehumidification cycle. The calculation of the ERH of AS in an organic-inorganic

180 solution is thermodynamically related to the solubility limit, but it is not strictly deterministic (unlike the

181 DRH) due to the stochastic nature of nucleation-and-growth of a crystal embryo. The molality of pure

182 AS at saturation in an aqueous solution is known, e.g. measured by Apelblat (1993) at 298.15 K as

183 $m_{AS}^{(sat)}$ = 5.790 mol/kg, while measurements are most often not available for the solubility limit of AS in

184 aqueous inorganic-organic systems. However, crystalline AS in equilibrium with an aqueous mixture

185 demonstrates a specific molal ion activity product (IAP) in that solution at a given temperature and

186 atmospheric pressure. For example, in the case of a ternary liquid mixture of levoglucosan + AS + water

187 in solid-liquid equilibrium (SLE) with a crystalline AS phase at a certain temperature T, a constant molal

188 ion activity product $IAP_{AS} = IAP_{AS}^{(sat)}(T)$ is established (necessary SLE condition). In this case the liquid

189 mixture is a so-called saturated solution with respect to AS. While the molar amount of AS in a saturated

190 solution depends on the other mixture constituents, the value of $IAP_{AS}^{(sat)}(T)$ is a function of temperature

191 only, since it is derived from the fixed chemical composition and associated chemical potential of the

192 crystalline phase. A reference value for $IAP_{AS}^{(sat)}(T)$ can therefore be calculated with the AIOMFAC

193 model from an experimentally determined solubility limit of AS in a known mixtures, such as the

194 molality of AS at the point of saturation in the binary aqueous system (water + AS). The RH at which

195 full dissolution of a solid phase upon humidification is just reached, the DRH, is directly related to the

196 conditions at which a saturated solution becomes subsaturated upon addition of water. Here the degree

197 of saturation with AS can be determined unambiguously by the computed value of IAP_{AS} as a function

198 of mixture composition and temperature. Making use of these thermodynamic relationships, the

199 AIOMFAC-based equilibrium model is used to calculate the DRH and ERH of AS in the multicomponent

200 system, as outlined below. Detailed information on the modeling of solid-liquid equilibria and the IAP-

201 based prediction of ERH is given in Zuend et al. (2011) and Hodas et al. (2016). Briefly, the ERH is

202   determined based on the following equations:

203    $$\text{IAP}_\text{AS} = \left[a^{(m)}_{NH_4^+}\right]^2 \left[a^{(m)}_{SO_4^{2-}}\right]^1 \tag{1}$$

204    $$\text{IAP}^{[\text{crit}]}_\text{AS} = c_\text{AS} \times \text{IAP}^{(\text{sat})}_\text{AS} \tag{2}$$

205   Here $a^{(m)}_{NH_4^+}$ and $a^{(m)}_{SO_4^{2-}}$ are the molal activities of the ammonium and sulfate ions in solution (Zuend et

206   al., 2010). Molality basis is indicated by superscript "(m)" (which is not a mathematical exponent).

207    $\text{IAP}^{(\text{sat})}_\text{AS}$ denotes the molal ion activity product of AS at salt saturation computed by the thermodynamic

208   equilibrium model for any aqueous AS system at a certain temperature (here 298.15 K). The calculated

209   molal IAP at saturation of the corresponding binary salt solution is taken as the (known) reference value.

210   The RH at which this $\text{IAP}^{[\text{sat}]}_\text{AS}$ value is just reached in certain bulk solution at equilibrium with its

211   environment (in contrast to $\text{IAP}_\text{AS} < \text{IAP}^{(\text{sat})}_\text{AS}$ at higher RH), is the (bulk) DRH of AS. Similarly, the ERH

212   is determined at the point of crystallization by a critical IAP value denoted as $\text{IAP}^{[\text{crit}]}_\text{AS}$ (Hodas et al.,

213   2016), the value of $\text{IAP}^{[\text{crit}]}_\text{AS} > \text{IAP}^{[\text{sat}]}_\text{AS}$ expresses the need for reaching a critical IAP threshold (critical

214   level of AS super-saturation) for highly likely nucleation-and-growth of a new crystalline AS phase. The

215   multiplication factor c_AS is used as a constant coefficient relating the IAP at AS saturation to the one

216   expected at the point of crystallization in aqueous mixed particles. From the comparison of laboratory

217   measurement of ERH for aqueous AS solution to the AIOMFAC-predicted IAP_AS at that RH, the value

218   of $c_\text{AS} \approx 30$ was determined; this value is in particular applicable to submicron-sized AS droplets (Zardini

219   et al., 2008; Ciobannu et al., 2010).

220   An analogous approach is used for the ERH predictions with the E-AIM model, however, since E-AIM

221   provides activity coefficients and activities on mole fraction basis, denoted here by superscript "(x)"

222   (rather than molality basis), the value of $c^{(x)}_\text{AS}$ need to be determined separately for that model.

223   Expressing Eq. (1) by mole-fraction-based activities of NH_4^+ and SO_4^{2-} and comparison to the

224    $\text{IAP}^{(\text{sat},x)}_\text{AS}$ and $\text{IAP}^{(\text{crit},x)}_\text{AS}$ computed by E-AIM for AS at the experimental solubility limit and ERH in

225   aqueous AS solutions, a value of $c^{(x)}_\text{AS} \approx 40$ was determined for the calculation with E-AIM.

226   As discussed by Lei et al. (2014), predicting of hygroscopic growth factors with E-AIM includes a

227   sophisticated composition-dependent solution density model, which considers the non-ideality effects on

228   apparent molar volumes used for the calculation of the solution density in mixed organic-inorganic

229 systems (Clegg and Wexler, 2011a, b). The AIOMFAC-based model applies a simpler solution density

230 treatment by assuming that the partial molar volumes of solution species are independent of non-ideal

231 interactions, i.e. the mixed solution density is calculated based on linear additivity of pure component

232 solid or liquid volume contributions to obtain the HGF at a given RH. Differences in the density models

233 are expected to lead to relatively small differences, typically on the order of the HTDMA measurement

234 error or less (e.g. Fig. 2a), in the application to HGF predictions, as demonstrated by Lei et al. (2014) for

235 the case of diameter vs. mass-based HGF of AS droplets. Both models include sophisticated sets of

236 equations to compute activity coefficients of all solution components in a thermodynamically consistent

237 manner.

238 2.4 *κ*-Köhler theory and computation of the hygroscopicity parameter *κ*

239 The hygroscopicity parameter, κ, is commonly used to characterize the relative hygroscopicities of

240 individual aerosol particles, known mixtures or complicated atmospheric aerosols (Petters and

241 Kreidenweis, 2007), and to model the composition-dependence of the solution water activity. The

242 saturation ratio, S, in the traditional Köhler equation (Eq. 3), over an aqueous droplet is calculated from

243 $$S = a_w \left(\frac{4\sigma_s M_w}{RT\rho_w D_{wet}} \right)$$ (3)

244 Where a_w is the mole-fraction-based water activity in solution, M_w and ρ_w are the molar mass of water

245 and the density of pure water in the liquid state at temperature T, respectively. D_{wet}, the "wet" particle

246 diameter at a given RH, is defined by $D_{wet} = HGF \times D_0$. D_0 denotes the diameter at dry conditions at

247 RH below 5 %. The solution surface tension is denoted by σ_s. In the "*κ*-Köhler theory", the bulk solution

248 water activity is described by a single parameter κ, with the hygroscopic parameter of the overall mixture

249 related to Eq. (3) by

250 $$\kappa_{HGF} = 1 - HGF^3 + \frac{HGF^3 - 1}{S} \exp\left[\frac{4\sigma M_w}{RT\rho_w D_{wet}}\right]$$ (4)

251 This expression describes effective values of κ_{HGF} as a function of droplet diameter and HGF at a

252 certain saturation ratio. In turn, known (measured) solution κ_{HGF} values or component-specific κ_i

253 values can be used to parameterize or predict the HGF curve of a mixture (Petters and Kreidenweis,

254 2007).

255 **2.5 GF data fit**

256 As described by Dick et al. (2001), the relationship between measured hygroscopic growth factors and

257 water activity can alternatively be parameterized by the following expression:

258 $$HGF = \left[1 + (c_1 + c_2 \times a_w + c_3 \times a_w^2)\frac{a_w}{1-a_w}\right]^{\frac{1}{3}} \qquad (5)$$

259 By substitution of Eq. (3) for a_w in Eq. (5) and a fit to the measured HGF the three adjustable coefficients

260 c_1, c_2, c_3 of Eq. (5) were determined. The coefficient values are given in Table 3 for the different

261 organic compounds considered.

262 **2.6 GF prediction by ZSR**

263 The Zdanovskii-Stokes-Robinson mixing rule is widely used to approximate the water uptake of mixed

264 systems by assuming additivity of the water uptake of each individual component in the mixed particles

265 at a given RH (e.g., Malm and Kreidenweis, 1997). HGF_{mix} is based on the HGF_j of pure components j

266 and their corresponding volume fraction, ε_j in the mixed particles.

267 $$HGF_{mix} = \left[\sum_j \varepsilon_j \left(HGF_j\right)^3\right]^{\frac{1}{3}} \qquad (6)$$

268

269 **3. Results and discussion**

270 **3.1 GF of single compounds systems**

271 Figure 2a shows the measured diameter growth factors of AS particles as a function of RH for both

272 humidification and dehumidification conditions. The measured ERH of 100 nm AS particles is

273 approximately 35 % RH at 298.15 K. The models predicted GF and predicted solid-liquid phase transition

274 of AS are in relatively good agreement with the experimental data and, in particular, the efflorescence

275 (crystallization) of AS is captured by the AIOMFAC and E-AIM models. The good model-measurement

276 agreement for the ERH is of course expected, since the aqueous AS system serves as the reference system

277 for determining the value pairs of $IAP_{AS}^{(sat)}$ and c_{AS} on molality and mole fraction basis for use with

278 AIOMFAC and E-AIM, respectively (section 2.3). An ERH of 31 % to 40 % RH was reported by other

279 groups for a range of particle sizes and experimental techniques (Zardini et al., 2008; Ciobanu et al.,

280   2010). There are several factors that contributed to the variability of reported ERH values, such as

281   particles size, temperature, solution impurities and the stochastic nature of the homogeneous or

282   heterogeneous nucleation of a crystalline phase near ERH (Ciobanu et al., 2010).

283   In Fig. 2b, upon dehydration, no efflorescence of the levoglucosan aerosol particles is observed even

284   at RH below 10 %. The agreement of the HGF between the hydration and dehydration processes

285   demonstrates that these particles equilibrate with the surrounding water vapor under these moisture

286   conditions. For example, the measured diameter growth factors of levoglucosan particles at 80, 60, and

287   30 % RH are 1.19, 1.09, and 1.03, respectively, which are similar to results obtained for the hydration

288   process of such particles. Levoglucosan has a DRH of ~80 % to 83 % (for a bulk system) at 293 to 298 K

289   (Mochida and Kawamura, 2004; Zamora et al., 2011). The similarity of diameter growth factors both

290   under hydration and dehydration conditions even below the DRH of levoglucosan is explained by the

291   lack of crystallization of levoglucosan upon drying to low RH and the presence of a metastable

292   supersaturated aqueous levoglucosan solution in both the hydration and dehydration modes for

293   experiments initiated with liquid solution droplets (Mochida and Kawamura, 2004; Chan et al., 2005;

294   Svenningsson et al., 2006). A possible reason for a persistent metastable supersaturated solution states is

295   that levoglucosan particles remain liquid (possibly a viscous liquid state) upon drying to below 5 % RH,

296   which was also observed previously with a reported ERH < 4% RH (Mochida and Kawamura, 2004;

297   Chan et al., 2005). Also, the measured diameter growth factors of levoglucosan particles are in good

298   agreement with these estimated from the standard UNIFAC model within the E-AIM model and the

299   AIOMFAC model, within experimental uncertainty. The UNIFAC models within E-AIM and AIOMFAC

300   are based on the original model expressions by Fredenslund et al. (1975) and both include the extensive

301   parameter set by Hansen et al. (1991) as well as revised parameters for certain group interactions of water

302   with carboxyl and hydroxyl groups by Peng et al. (2001). Of relevance for levoglucosan and other sugar-

303   like compounds, the AIOMFAC model also contains certain revised group parameters for hydroxyl

304   groups and special alkyl groups for their interactions with water, introduced by Marcolli and Peter (2005)

305   for polyols, as further detailed in Zuend et al. (2011). However, the molecular structure of levoglucosan

306   with several polar functional groups in close vicinity may account for a small deviation between models

307   and measured *HGFs* at RH below 70 %, because intramolecular interactions are not fully considered by

308   these models.

309   The measured diameter growth factors of 4-hydroxybenzoic acid particles shown in Fig. 2c

310   demonstrate untypical increase in diameter of 4-hydroxybenzoic acid particles during dehumidification

311   from 90 to 10 % RH, which is consistent with previous diameter growth factor for a few solid particles

312   (Mochida and Kawamura, 2004). The organic particles measured are likely always in the effloresced, i.e.

313   crystalline state apparently even at high RH. The apparent increase in diameter during dehumidification

314   may be explained by particle shape restructuring, since the (poly)-crystalline particles are likely non-

315   spherical at dry conditions, but may become more sphere-like in shape when exposed to higher RH

316   (Mikhailov et al., 2004). Also, no ERH of 4-hydroxybenzoic acid in the dehydration mode was observed

317   during the experiments; the likely reason is that the highest RH reached in the humidifier was

318   approximately 98 %, which may be below the ERH of 4-hydroxybenzoic acid, reported as above 98 %

319   RH in another study (Mochida and Kawamura, 2004). As discussed previously by Lei et al. (2014), our

320   HTDMA experiments are carried out such that RH = 98 % is reached initially before dehumidification

321   to a series of relative humidities at set point RH2 (90 % – 5 % RH), the crystallization of the organic,

322   however, could occur at above 90 % RH. In addition, deviations between measurements and model

323   prediction are obvious in Fig. 2c. The observations surpass by far the expected error in model

324   performance, which is typically less than 0.05 in HGF units for RH < 85 %, as indicated also by an

325   intercomparison of the AIOMFAC and E-AIM predictions in Fig. 2c and much improved model-

326   measurement agreement for the case of mixed 4-hydroxybenzoic acid + AS particles shown in Fig. 4

327   (discussed in Section 3. 2. 2). However, note that the validity of the shown model predictions in Fig. 2c

328   depends on whether the assumption of a liquid solution droplet is plausible. Therefore, it is no surprise

329   that the model-predicted curves deviate from the experimental hygroscopic behavior of 4-

330   hydroxybenzoic acid particles. Morphology effects, such as the restructuring of non-spherical

331   polycrystalline particles over a certain RH range or liquid-liquid phase-separated particles of non-

332   spherical shapes, have been discussed by several groups (Sjogren et al., 2007; Reid et al., 2011; Lei et

333   al., 2014). In the case of hygroscopic growth and deliquescence under hydration conditions for 4-

334   hydroxybenzoic acid particles and mixtures of 4-hydroxybenzoic acid with ammonium sulfate. An offset

335   between measurement and model predictions was observed both in the RH range below the deliquescence

336   of the particles and above it, i.e. above 80 % RH, (Lei et al., 2014). It is suggested that deviations are

337   primarily caused by a change in solid-state particle morphology during hydration, leading to a

338   restructuring of the polycrystalline particle shape towards more compact, near-spherical shape as the RH

339 approaches the particle deliquescence point. This would explain rather uncommon HGF values of less

340 than 1.0 at elevated RH also shown in Fig. 2c. Similar behavior was found for experimental growth

341 factors of mixtures containing adipic acid and AS and systematic deviations between the associated ZSR

342 predictions and observations by Sjogren et al. (2007). Thus, while experimental data hint to the possible

343 influence of non-spherical particles and their humidity-induced restructuring as a source of uncertainty,

344 model predictions of HGF, such as those with the AIOMFAC model, assume by default a spherical

345 particle shape even for solid phases and/or in cases where LLPS is present.

346   The measured HGF curves of humic acid aerosol particles during dehumidification and humidification

347 measurements do not agree very well within experimental uncertainty, in particular above 70 % RH. For

348 instance, the growth factor of humic acid aerosol particles at 80 % RH is 1.2 according to the

349 dehumidification measurement, which is higher than hygroscopic growth factor of humic acid particles

350 in the humidification mode at the same RH. Humic acid aerosol particles shrink continuously due to loss

351 of water content in the range from 90 % to 10 % RH. For example, a stepwise change in the water

352 absorption and desorption behavior within different RH range was observed in the case of Nordic Aquatic

353 Fulvic Acid (NAFA) and Suwannee River Fulvic Acid (SRFA) by Chan and Chan (2005). These

354 hygroscopic behaviors suggest that humic acid particles and structurally similar compounds remain some

355 water down to the low RH levels achieved in the instruments (imperfect drying during particle residence

356 in the instrument). In addition, the experimental growth factor of humic acid aerosol particles during

357 dehumidification can be represented well by fitting Eq. (5) to the measurements. The determined fit

358 parameters are listed in Table 3. The humic acid sample used (Aldrich, 99%) are a mixture of different

359 poly-carboxylic acids of undefined chemical structure. However, specific information on the chemical

360 structure and mixture composition is necessary for corresponding model predictions with AIOMFAC and

361 E-AIM. Therefore, no such model calculations are shown in Fig. 2d.

362 **3.2 GF of mixtures of organic surrogate compounds + ammonium sulfate**

363 Biomass burning aerosol particles are likely mixtures of a diversity of inorganic constituents and organic

364 compounds in the atmosphere. For example, particles may consist of a combination of ammonium sulfate

365 mixed with low- and semi-volatile organics from biomass burning emissions (Lee et al., 2003; Zhang et

366 al., 2007; Pratt and Prather, 2010). Different water solubilities, and hygroscopic behavior of distinct

367　　organic compounds may affect the hygroscopic growth factors of mixtures of partially or fully dissolved

368　　inorganic and organic components. For example, Bodsworth et al. (2010) studied the effect of different

369　　mass fractions of citric acid on the efflorescence properties of mixed citric acid-ammonium sulfate

370　　particles at lower temperature and concluded that adding citric acid decreases the ERH of ammonium

371　　sulfate in the mixed aerosol particles. These hygroscopic behaviors of mixed aerosol particles, including

372　　phase transition in the range from moderate to low RH, are the focus of attention in this study.

373　　**3.2.1 Mixed system: levoglucosan + ammonium sulfate**

374　　Figure 3 shows measured growth factors of mixed aerosol particles containing levoglucosan +

375　　ammonium sulfate with different dry state organic-to-inorganic mass ratios (1:3, 1:1, 3:1) in the RH range

376　　from 90 % to 10 %. There is a reduction in the diameter growth factor of aerosol particles containing

377　　levoglucosan and AS with increasing levoglucosan mass fraction, as expected from a ZSR-like additivity

378　　concept of hygroscopicity. When the concentration of levoglucosan is low (25 wt %), a clear

379　　efflorescence signature of AS found, within the ERH shifting to a higher RH (40 % - 45 %) in comparison

380　　to the ERH of pure AS occurring at 33 %-35 % RH (Fig.3a). A similar phenomenon has been found for

381　　the certain mixtures of NaCl and Nordic Aquatic Fulvic Acid (NAFA), in which the crystallization of

382　　NaCl shifted to higher RH by mixing with NAFA at a mass ratio of 1:1 (Chan and Chan. 2003). With

383　　increasing mass fraction of levoglucosan (i.e., 50 wt % and 75 wt %), the mixtures release water gradually

384　　and no crystallization of AS was observed. Although a small step in the growth factor curve might have

385　　occurred (indicative of the crystallization of AS), it cannot be detected with sufficient certainty by our

386　　measurement setup. The rather high viscosity of solutions containing levoglucosan is expected to

387　　increase considerably toward RH (Marshall et al., 2016). This increase in viscosity might impede the

388　　crystallization of AS in the mixed systems on the time scale of the experiment. Mass transfer limitation

389　　effects on the deliquescence or efflorescence process of crystalline organic particles and the water uptake

390　　or evaporation have been investigated in several experimental studies (Peng et al., 2001; Choi and Chan,

391　　2002; Chan and Chan, 2005; Sjogren et al., 2007; Zardini et al., 2008; Ciobanu et al., 2010; Smith et al.,

392　　2012; Mikhailov et al., 2013; Hodas et al., 2015). Mass transfer limitations may impact the outcome of

393　　experiments significantly if the characteristic time scales for equilibration is similar to or larger than the

394　　residence time of particles in the experimental setup. In this study, the total residence time of the aerosol

395　　sample during the equilibration phase before entering the DMA2 is about 8 s. In order to improve the

396   probability that the particles reach equilibrium with the target RH during this residence time, the

397   monodisperse aerosol selected by DMA1 is first humidified to 98 % RH. The aerosol particles are then

398   exposed to a lower target RH by a two-step process using double Nafion tubes. Kerminen (1997)

399   estimated the necessary residence time for achievement of water equilibrium of aqueous droplets to be

400   between 8 ×10-6 s and 0.1 s for 100 nm and 500 nm particles, respectively. Therefore, the typical

401   residence time of a few seconds in the humidification or dehumidification section in a HTDMA

402   measurement is assumed to be sufficient for most equilibrium hygroscopicity measurements (Brooks et

403   al., 2004; Mikhailov et al., 2004). Moreover, our HGF results for the three pure organic components are

404   in good agreement with respective data by Mochida and Kawamura, (2004), Brooks et al., (2004) and

405   Chan and Chan (2005) conducted with different techniques and/or residence times. However, there are

406   cases where water equilibration could be impeded substantially in the presence of highly viscous or

407   glassy particles at low RH, e.g. for ternary sucrose + NaCl + water particles of > 6 μm in diameter studied

408   by Bones et al. (2012), who report an equilibration time scale > 1000 s for such particles. Note that, aside

409   from viscosity, there is an important size-dependence of the particles on the equilibration time scale (e.g.

410   Koop et al. 2011). For aqueous 100 nm particles used in HTDMA experiments at room temperature,

411   Bones et al. (2012) indicate that the equilibration time scale for water is likely only of concern for RH <

412   10 % in such an instrument. We therefore conclude that the residence time of 8 s is very likely sufficient

413   to allow for equilibrium HGF measurements in dehydration mode, at least down to 10 % RH (when

414   starting with aqueous solution droplets).

415   Mass transfer effects in hygroscopicity measurements of aerosol particles during hydration conditions

416   have been encountered previously, particularly when a solid-liquid phase transition (deliquescence) is

417   involved (Peng et al., 2001; Chan and Chan, 2005; Sjogren et al., 2006). For example, Peng et al. (2001)

418   observed in electrodynamic balance (EDB) experiments under conditions of very slow humidification

419   that glutaric acid aerosol particles showed a deliquescence phase transition in the RH range from 83 to

420   85 % over the course of several hours. This is a much longer time span than that of ~ 40 min for the

421   deliquescence of other super-micron sized dicarboxylic acid particles (e.g., malonic acid) in EDB

422   experiments. This observation indicates that the solid-liquid phase transition of glutaric acid particles

423   may likely be mass transfer limited during the hydration process. In this context, it is possible that the

424   deliquescence of initially solid, pure 4-hydroxybenzoic acid particles at RH > 97 % is further impeded

425 by slow dissolution, which could have led to the absence of deliquesced particles (Fig. 2c) on

426 experimental time scale.

427   In addition, the measured diameter growth factors of mixtures of levoglucosan and AS are compared

428 to calculations of hygroscopic growth by the E-AIM and AIOMFAC models. The E-AIM prediction is

429 in relatively good agreement with results from the HTDMA measurement but typically overestimates the

430 water content of particles consisting of organic-AS mixtures at the RH range close to the ERH of AS.

431 The liquid-solid phase transition of ammonium sulfate in the mixed particles is considered in the E-AIM

432 assumptions as described in Section 2.3. There is a more distinct shift of ERH of AS with higher mass

433 fractions of levoglucosan. In the case of the AIOMFAC and E-AIM model predictions, it is assumed that

434 the diameter growth factor contribution from AS is zero below the predicted ERH, i,e. there the growth

435 factor deviation from 1.0 is solely due to the organic water uptake. The model prediction shows a slight

436 deviation from the measurements, which may be in part due to (i) model uncertainty in the correct

437 description of the hygroscopicity of levoglucosan, (ii) due to incomplete representation of AS +

438 levoglucosan interactions in aqueous solutions and (iii) in part due to measurement error. Also, in the

439 case of mixtures consisting of AS and levoglucosan with organic-to-inorganic dry mass ratio of 3:1 (75

440 wt % levoglucosan of dry particle composition), the underestimation of the growth factor by the

441 AIOMFAC model at RH < 35 % in comparison to the measurements is explained in part by the model

442 prediction of AS efflorescence (which seems to be absent in the measurements). However, with

443 decreasing AS mass fraction, the hygroscopic behavior of levoglucosan dominates the diameter growth

444 factors of the mixtures, in relative agreement with the AIOMFAC-modeled "dehydration branch"

445 prediction. Minor differences in the AIOMFAC prediction vs. -measurement for diameter growth factors

446 of mixed levoglucosan and AS in the RH range of 35 - 25 % here might be attributed to mixture viscosity

447 effects at the higher levoglucosan contents, which may suppress the efflorescence of AS in the mixed

448 systems on experimental timescale or it could simply be due to sufficient miscibility of dissolved AS in

449 the aqueous levoglucosan solution (beyond that predicted by the model), such that a small step-change

450 due to AS efflorescence could be beyond the experimental detection range. As a result, accounting for

451 the effect of the organic components on the diameter growth factors of mixtures within aerosol particles

452 is crucial to model accurately the equilibrium hygroscopic behavior.

453 **3.2.2 Mixed system: 4-hydroxybenzoic acid + ammonium sulfate**

454   Mixtures of 4-hydroxybenzoic acid + AS with different organic mass fraction (25, 50, 75 wt %) exhibit

455   a gradual water desorption before the AS fraction of the particle effloresces at a certain RH. With

456   increasing 4-hydroxybenzoic acid mass fraction, no discontinuity step at the corresponding ERH in the

457   dehydration curve of mixtures is observed. This suggests the presence of 4-hydroxybenzoic acid in the

458   liquid state retards or offsets the efflorescence of AS in the mixtures. An interesting, yet contrasting

459   phenomenon was observed for the hydration process of aerosol mixtures containing 4-hydroxybenzoic

460   acid and AS by Lei et al. (2014). For the case of these mixtures during moistening, the deliquescence of

461   ammonium sulfate in the mixed particles remains unaffected, within experimental resolution, by the

462   presence of 4-hydroxybenzoic acid (Lei et al., 2014). Similar behavior has been observed for particles

463   containing certain organic acids of limited water-solubility mixed ammonium sulfate (Choi and Chan,

464   2002; Chan and Chan, 2003). For example, mixtures for succinic acid + ammonium sulfate showed no

465   substantial influence on the deliquescence RH of ammonium sulfate in the hydration process (Choi and

466   Chan, 2002). However, a clear RH shift of the deliquescence phase transition of ammonium sulfate or

467   sodium chloride was determined for mixed particles containing organic acids of higher water-solubility

468   and O: C ratio, such as citric acid and malonic acid (e.g. Choi and Chan, 2002). The DRH and ERH of

469   pure organics and AS in the mixed organic-AS particles are summarized in Table 4, the measurements

470   indicate that 4-hydroxybenzoic acid has a significant effect on the efflorescence of AS when present in

471   sufficient amount. Also, there is a clear reduction in the diameter growth factors prior to crystallization

472   for mixtures with increasing 4-hydroxybenzoic acid mass fraction.

473   The measurements of mixtures consisting of 4-hydroxybenzoic acid and AS are compared with model

474   predictions based on different assumptions about the phase state of the organic component, since the

475   deviation from measurements might partly be explained by a transition in the physical state of the organic

476   component. The E-AIM model prediction is referring to a system where the mixtures of 4-

477   hydroxybenzoic acid is assumed to be in the liquid state at all RH levels, which the efflorescence of AS

478   is considered. Neglecting the potential efflorescence of the organic component in the dehydration branch

479   makes a systematic offset more obvious prior to the efflorescence of AS. A good E-AIM model-

480   measurement agreement occurs below the predicted ERH of AS for mixed particles. The overestimation

481   of HGFs before the efflorescence of AS is explained by the AIOMFAC model prediction with distinct

482   assumptions about the organic phase state. A possible reason for the departure of model-measurement

483   agreement at RH < 80 % is that there are two liquid-to-solid phase transitions, occurring in the mixed

484   particles: a gradual one for the organic component and a step-like one for AS at lower RH. This

485   phenomenon is shown in the grid square range in Fig. 4 and supported by comparison of the measured

486   HGF data with AIOMFAC-based predictions for two assumptions about the organic phase state,

487   especially in the case of mixtures with 50 and 75 wt-% organic. We acknowledge that the model

488   predictions of the HGF curves for the two organic phase state assumptions differ within experimental

489   error for the case shown in Fig. 4a, indicating that alternative explanations, such as model/measurement

490   uncertainty in the absence of a liquid-solid phase transition could explain the observations. In the Fig.

491   4b, good agreement between measurements and the AIOMFAC model prediction with liquid organic

492   assumption is found for RH > 65 %, while for RH ≤ 60 % the experimental data agree very well with the

493   dashed red model curve for the case with consideration of a solid organic component. It suggests that

494   crystallization followed by gradually increasing partitioning of organic from the solution to the solid

495   organic phase occurs in the range from 70 % to 60 % RH under conditions of dehumidification. Similarly,

496   a liquid-to-solid phase transition occurs for the organic: AS mass ratio of 3:1 cases in the range from 80 %

497   to 50 % RH. Meanwhile, AS remains dissolved in a supersaturated aqueous solution phase. Moreover,

498   the AIOMFAC-based equilibrium model predicts a liquid-liquid phase separation (LLPS) to occur at RH

499   below ~ 90 % for the calculation cases with the assumption of the organic in the liquid state (for all three

500   organic mass fractions in Fig. 4). This prediction leads to a liquid phase enriched in 4-hydroxybenzoic

501   acid with some water and AS dissolved and a coexisting liquid phase enriched in AS and water. The onset

502   of the LLPS during dehumidification leads to the kink in the red model curve near 90 % RH, since the

503   slope of the HGF curve with RH changes in a non-smooth manner at the point of the LLPS phase

504   transition. This change in slope is not noticeable from the experimental data alone, but the model-

505   measurement comparison for the range above 80 % RH shows very good agreement. The two liquid

506   phases will likely remain separated until nucleation of a crystalline 4-hydroxybenzoic acid phase occurs

507   followed by gradual partitioning of the organic acid to the solid phase with decreasing RH (to ~50 %

508   RH), at which point only a single liquid phase (an aqueous AS phase with a tiny amount of dissolved

509   HA) will remain until efflorescence of AS occurs. Above ~90 % RH, a single, homogeneous liquid phase

510   is predicted to exist. Interestingly, this AIOMFAC model-measurement comparison (Fig. 4, especially

511   panels b and c) provides reasonable evidence that 4-hydroxybenzoic acid remains dissolved and therefore

512   in a liquid phase state at high RH in the mixed particles upon dehumidification (it is present in both liquid

513   phases below 90 % RH, but highly enriched in the AS-poor phase). In contrast, in the case of pure 4-

514   hydroxybenzoic acid aerosol particles, particles exposed to initial RH of $\geq$ 90 % remain in the solid state

515   (or crystallize at RH > 90 %) in the dehydration mode (Fig. 2c). What factors contribute to keeping the

516   organic in the liquid solution? It is possible that the aerosols generated with those mixed solutions were

517   allowing the 4-hydroxybenzoic acid to fully dissolve as the AS provides substantial particle phase water

518   content (within short time) into which the organic can be dissolved and may then further contribute to

519   water uptake associated with the organic's hygroscopicity (unlike in the case of the pure 4-

520   hydroxybenzoic acid particles). The 4-hydroxybenzoic acid remains dissolved in the mixture, possibly

521   supersaturated with respect to the crystalline organic state (similarly to how AS stays supersaturated at

522   RH below the DRH during drying). We consider this a reasonable explanation for the observed HGF data

523   from the HTDMA in comparison to the different AIOMFAC-based curves.

524   **3.2.3 Mixed system: humic acid + ammonium sulfate**

525   Figure 5 shows that the experimental diameter growth factors of mixtures consisting of humic acid (HA)

526   and AS with dry mass ratios of 1:3, 1:1 or 3:1 decreases with increasing mass fraction of HA at RH >

527   35 %. For example, at 35 % RH the measured HGF are 1.1, 1.05, 1.05 for the particles consisting of 25

528   wt %, 50 wt % and 75 wt % humic acid. In comparison, the diameter growth factor of pure supersaturated

529   AS particles is ~ 1.13 just prior to efflorescence of AS. Humic acid, unlike levoglucosan and 4-

530   hydroxybenzoic acid aerosol particles, has no noticeable effect on the efflorescence point of AS in the

531   mixed aerosol particles. Results of the ZSR model agrees well with measured hygroscopic growth for

532   mixtures within the experimental error. The ZSR curves shown in Fig. 5 are based on the RH-dependent

533   fitted hygroscopic growth factors of humic acid with Eq. (5) and the AIOMFAC predicted diameter

534   growth factors of AS in the dehydration mode. The success of the ZSR mixing rule for this system

535   suggests that interactions of organic molecules with ammonium sulfate ions in aqueous solution will only

536   marginally affect the hygroscopic growth factors of the mixtures containing humic acid and AS. Due to

537   the lack of detailed information about the actual chemical structures of humic acid samples used, it was

538   not possible to perform E-AIM and AIOMFAC model predictions for comparison with the measurement.

539   **3.3 Mixtures of biomass burning organic surrogate components with ammonium sulfate**

540   According to Decesari et al, (2006), sampling of aerosol particles, including the WSOC fraction, was

541   conducted from September 9 to November 14, 2002 in their field study, the sampling time was subdivided

542   into different periods. Despite of significant changes in the chemical composition of tracer compounds

543   from the dry to the wet period, the functional groups and general chemical classes of WSOC changed

544   only to a small extent in the Amazon basin near Rondônia, Brazil. Model compounds represent semi-

545   quantitatively (presence/abundance of functional groups) and the chemical structure of WSOC can be

546   used as surrogates in microphysical models involving organic aerosol particles over tropical areas

547   affected by biomass burning scenarios (Andreae et al., 2002; Artaxo et al., 2002; Rissler et al., 2006;

548   Decesari et al., 2006). Here, we focus on experimental observations and model calculations for relatively

549   simple mixtures of inorganic-organic surrogate components reflecting mixtures of aerosol components

550   found during different seasons during biomass burning events. However, we are fully aware of that fact

551   that actual biomass burning aerosols are typically much more complex in terms of particle chemical

552   composition. Aerosol particle properties from biomass burning events depend on the types of sources,

553   external/internal population mixing state, water-solubilities, and phase state of the diversity of organic

554   compounds and their mixing with inorganic constituents during different time periods in the field (e.g.

555   Decesari et al., 2006).

556   **3.3.1 Mixtures system: mix-bio-dry and mix-bio-wet aerosol particles**

557   Figure 6a shows the observed small differences in the hygroscopicity parameter κ for mixtures of organic

558   surrogate components and ammonium sulfate representing biomass burning particles during the dry and

559   wet periods in the Amazon, respectively. Hygroscopicity parameter values for bio-mix-dry aerosol

560   particles were determined to be between 0.16 and 0.18 with decreasing RH in the range from 90 % to

561   40 % RH. The κ value representing the wet period in the Amazon is shown in Fig. 6b, derived from

562   laboratory HTDMA measurements in the range from 90 % to 40 % RH. A similar trend of an increase in

563   κ with a decrease in RH has also been observed by Cheung et al. (2015). Their observation is based on

564   ambient particle measurement with a HTDMA in Hong Kong, therefore probing particles of more

565   complex compositions in the field campaign. The variability of the hygroscopicity parameter in sub-

566   saturated conditions reveals some limitations of a single-parameter hygroscopicity model for applications

567   over a wide range of RH. At low, intermediate and high RH levels, differing degrees of solution non-

568   ideality, potential for liquid-liquid phase separation, water-solubility limitations of organics in ambient

569   organic-inorganic particles, and assumptions about constant/variable surface tension may all play a role

570 (Mikhailov et al., 2009; Wex et al., 2009, Rastak et al., 2017; Ovadnevaite et al. 2017; Wang et al., 2017).

571 In the case of κ of organic surrogates mixed with ammonium sulfate, the relevant κ value range is ∼ 0.12

572 to 0.15 obtained from 90 % to 40 % RH. The measured κ values of the mixtures are compared to field

573 data of HTDMA and CCN measurements conducted at a remote rainforest site in the central Amazon

574 during the dry and wet seasons (Whitehead et al., 2016; Pöhlker et al., 2016), which are consistent with

575 κ obtained at similar field sites (within the uncertainty of experiments). The likely reason for a relatively

576 good agreement between the hygroscopicity of the laboratory mixtures and the field data is that the

577 organic mass fractions of the mix-bio-dry and mix-bio-wet mixtures are chosen in our laboratory

578 experiments to be similar to those of the latest field data from Amazon. For example, Pöhlker et al. (2016)

579 obtained the effective hygroscopicity parameters κ between 0.3 ± 0.01 and 0.15 ± 0.01 based on the

580 organic mass fraction range from 0.65 to 0.97 in the dry season by aerosol chemical speciation monitor

581 (ACSM) and CCN measurements. The predicted κ values of the mixtures at various RH levels shown in

582 Fig. 6 (black curves) are obtained by application of Eq. (4) with use of the RH-dependent fitted HGFs of

583 the organic surrogates (Eq. 5), the predicted growth factor of AS by the AIOMFAC model (for the

584 humidification case) and the volume fraction based mixing rule for a mixture's HGF (Eq. 6). For these

585 calculations, a solution surface tension of 0.072 J m^{-2} was assumed. These predictions agree relatively

586 well with the experimental κ_{dry} and κ_{wet} values obtained from the HTDMA over a wide range in RH

587 referring to dehumidification conditions (no solid AS). Furthermore, the combined approach of Eqs. (4-

588 6) allows for a prediction of the change in κ at high RH towards water vapor super-saturation. A small

589 difference in κ between sub- and super-saturated conditions is observed for our mixed systems when

590 comparing the HTDMA data and predictions at 90 % RH with the predictions near 100 % RH and the κ

591 values from the CNN field measurements. The difference is more pronounced for the wet season case.

592 Rastak et al. (2017) observed a marked difference in apparent hygroscopicity and related mixture κ of

593 the organic aerosols (AS-free) occurring in the case of monoterpene-derived secondary organic aerosol

594 (SOA) for sub- vs. super-saturated conditions. A smaller difference was reported for the isoprene-derived

595 SOA (Pajunoja et al., 2015: Rastak et al., 2017), more like the difference observed here for the mixtures

596 containing AS (and therefore having overall higher κ values than typical salt-free organic aerosols).

597 Rastak et al. (2017) attribute the distinct difference in κ_{SOA} of the monoterpene SOA to the limited mutual

598 solubility of certain SOA components in water, because a single liquid organic-phase of monoterpene

599 oxidation products is present at RH below 95 %, but over a RH range above 95 %, liquid-liquid phase

600 separation is observed by optical microscopy as well as predicted by the AIOMFAC-based equilibrium

601 model. In the mix-bio-wet and mix-bio-dry cases shown in Fig. 6, the likely reason for the change in

602 characteristic mixture hygroscopicity is not necessarily due to a liquid-liquid phase separation at high

603 RH. For example, the κ parameter obtained from field data is ~0.15±0.06 at 90 % RH, while its value

604 reaches ~0.18±0.04 at RH > 100 % (just prior to CCN activation). A likely reason for the difference is

605 that hygroscopic particles, especially those containing sparingly soluble organics like 4-hydroxybenzoic

606 acid, take up water dramatically above 95 % RH when approaching 100 % RH (Huff Hartz et al., 2006;

607 Chan et al., 2008; Rastak et al., 2017), which is clear from model predictions, as demonstrated in Fig. 6

608 by application of Eq. (4). The predicted curve in the mixture's effective κ parameter may well capture

609 the change in hygroscopicity under such high RH conditions. Consequently, for a precise representation

610 of the hygroscopic growth behavior (e.g. HGF) at high RH (> 95 %) by the κ-Köhler model, the value of

611 κ would need to be varied. While a variable κ value is contrary to the attempted simplicity of the single-

612 parameter κ-Köhler model, it is at least advised to consider that κ values derived from HGF data at 80 %

613 or 90 % RH may not apply accurately for the calculation of CCN activation properties of such biomass

614 burning aerosols.

615　　To summarize, there is small difference in hygroscopicity parameters between sub-saturated

616 measurement conditions at 90 % RH in the laboratory with HTDMA and supersaturated conditions using

617 CCN measurements, in agreement with the findings of other studies. At regional scale, in the dry and wet

618 period, the hygroscopic behavior in some extent of the Amazon rainforest is influenced significantly by

619 the biomass burning emissions, which enhances CCN activity and droplet number concentrations in

620 warm clouds in that region and influences the radiation balance and cloud life time (Pöschl et al., 2010).

621 Underestimation of organic surrogate component mass fractions in the mixed particles or organic:sulfate

622 mass ratios may be responsible for the slight differences in the determined κ parameters of the laboratory

623 and field measurements.

624

625 **4. Conclusions**

626 A number of field-based hygroscopicity studies about biomass burning aerosol focus on the growth

627 factors of mixtures at high RH (e.g. 90 % RH). However, less attention has been paid to the growth

628   behavior at low to moderate RH, limiting the database for accurate estimates of particles optical and

629   radiative properties over those lower RH ranges. However, this is a RH range in which water uptake or

630   release behavior demonstrates a considerable variability among different organic-inorganic systems. The

631   occurrence or suppression of a liquid-solid phase transition affects the physicochemical particle

632   properties in a relative narrow RH range, potentially leading to particles of different morphology and

633   physical states, affecting effective particle size and density. In this work, measurements and

634   thermodynamic equilibrium predictions for organic-inorganic aerosols related to components from

635   biomass burning emissions demonstrate a diversity of hygroscopic growth/shrinking behavior. For

636   example, in the case of aerosol mixtures containing levoglucosan and ammonium sulfate, the presence

637   of levoglucosan may cause the efflorescence of AS to occur at higher RH than in pure aqueous AS

638   particles-or it may completely suppress AS efflorescence, as observed for mixtures with a high

639   levoglucosan mass fraction. The growth curves predicted with an AIOMFAC-based thermodynamic

640   equilibrium model reproduce the observations in most cases reasonably well and we demonstrate the

641   usefulness of predictions with different assumptions about the physical state of the organic components

642   for the interpretation of experimental data, such as in the case of mixtures of 4-hydroxybenzoic acid and

643   ammonium sulfate. However, the accurate prediction of AS efflorescence or its suppression in mixed

644   particles is difficult. The E-AIM-predicted growth curves reproduce the measured hygroscopic behavior

645   relatively well for the consideration of the effect of 4-hydroxybenzoic acid on the hygroscopic behavior

646   of mixtures with ammonium sulfate, which leads to suppression of the ammonium sulfate efflorescence.

647   In the case of mixtures of humic acid and ammonium sulfate, continuous water desorption of aerosol

648   particles shows no significant effect on the efflorescence of ammonium sulfate. Also, as expected, there

649   is a clear reduction in the diameter growth factor of mixed systems, in comparison with that of pure AS

650   particles. In addition, the small difference of hygroscopicity parameters of mix-bio-dry and mix-bio-wet

651   systems between measured data in the laboratory using HTDMA and the field using CCN activity

652   measurements is due to the similar O:C ratios of organic surrogate compounds and ammonium sulfate

653   mass fractions used in the model mixtures when experimental κ data from sub- and super-saturated water

654   vapor conditions are compared.

655   The range of measurement-model comparisons presented in this study indicate that providing accurate

656   thermodynamic model predictions of the hygroscopic growth behavior of mixed organic-inorganic

657   systems remains a challenging problem. At moderate and low RH, where aerosol solution phases become

658   highly concentrated, step-like or gradual crystallization and related solid-liquid equilibria may occur with

659   high sensitivity to the organic/inorganic mass ratio and the chemical nature of the mixture constituents.

660   To further improve thermodynamic equilibrium models for the prediction of hygroscopicity and phase

661   transitions, controlled laboratory experiments with single solutes and/or with mixed organic-inorganic

662   systems of known phase state will be useful to constrain model parameters. Ideally, such measurements

663   should cover the high, intermediate and low RH ranges under humidification and dehumidification

664   conditions.

665

674

675   **Reference**

676   Altaf, M. B., Zuend, A., and Freedman, M. A.: Role of nucleation mechanism on the size dependent

677   morphology of organic aerosol, Chemical communications, 52, 9220-9223, 2016.

678   Andreae, M. O. and Gelencser, A.: Black carbon or brown carbon? The nature of light-absorbing

679   carbonaceous aerosols, Atmospheric Chemistry and Physics, 6, 3131-3148, 2006.

680   Apelblat, A.: The vapour pressures of saturated aqueous solutions of potassium bromide, ammonium

681   sulfate, copper (II) sulfate, iron (II) sulfate, and manganese (II) dichloride, at temperatures from 283 K

682   to 308 K, The Journal of Chemical Thermodynamics, 25, 1513-1520, 1993.

683   Arnold, S., Emmons, L., Monks, S., Law, K. S., Ridley, D., Turquety, S., Tilmes, S., Thomas, J. L.,

684   Bouarar, I., and Flemming, J.: Biomass burning influence on high-latitude tropospheric ozone and

685   reactive nitrogen in summer 2008: a multi-model analysis based on POLMIP simulations, Atmospheric

686   Chemistry and Physics, 15, 6047-6068, 2015.

687   Artaxo, P., Martins, J. V., Yamasoe, M. A., Procópio, A. S., Pauliquevis, T. M., Andreae, M. O., Guyon,

688   P., Gatti, L. V., and Leal, A. M. C.: Physical and chemical properties of aerosols in the wet and dry

689   seasons in Rondônia, Amazonia, Journal of Geophysical Research: Atmospheres, 107, LBA 49-41-LBA

690   49-14, 2002.

691   Atkinson, D. B., Radney, J. G., Lum, J., Kolesar, K. R., Cziczo, D. J., Pekour, M. S., Zhang, Q., Setyan,

692   A., Zelenyuk, A., and Cappa, C. D.: Aerosol optical hygroscopicity measurements during the 2010

693   CARES campaign, Atmospheric Chemistry and Physics, 15, 4045-4061, 2015.

694   Bahadur, R., Praveen, P. S., Xu, Y. Y., and Ramanathan, V.: Solar absorption by elemental and brown

695   carbon determined from spectral observations, Proceedings of the National Academy of Sciences of the

696   United States of America, 109, 17366-17371, 2012.

697   Beyer, K. D., Friesen, K., Bothe, J. R., and Palet, B.: Phase Diagrams and Water Activities of Aqueous

698   Dicarboxylic Acid Systems of Atmospheric Importance, Journal of Physical Chemistry A, 112, 11704-

699   11713, 10.1021/jp805985t, 2008.

700   Bodsworth, A., Zobrist, B., and Bertram, A. K.: Inhibition of efflorescence in mixed organic-inorganic

701   particles at temperatures less than 250 K, Physical chemistry chemical physics : PCCP, 12, 12259-12266,

702   2010.

703   Bones, D. L., Reid, J. P., Lienhard, D. M., and Krieger, U. K.: Comparing the mechanism of water

704   condensation and evaporation in glassy aerosol, Proceedings of the National Academy of Sciences, 109,

705   11613-11618, 2012.

706   Boucher Olivier and David, R.: Clouds and Aerosols, PICC, 2013.

707   Brooks, S. D., DeMott, P. J., and Kreidenweis, S. M.: Water uptake by particles containing humic

708   materials and mixtures of humic materials with ammonium sulfate, Atmos. Environ., 38, 1859-1868,

709   2004.

710 Carrico, C. M., Petters, M. D., Kreidenweis, S. M., Collett, J. L., Engling, G., and Malm, W. C.: Aerosol

711 hygroscopicity and cloud droplet activation of extracts of filters from biomass burning experiments,

712 Journal of Geophysical Research, doi:10.1029/2007JD009274, 2008.

713 Chan, M. N. and Chan, C. K.: Hygroscopic properties of two model humic-like substances and their

714 mixtures with inorganics of atmospheric importance, Environmental Science & Technology, 37, 5109-

715 5115, 2003.

716 Chan, M. N., Choi, M. Y., Ng, N. L., and Chan, C. K.: Hygroscopicity of water-soluble organic

717 compounds in atmospheric aerosols: Amino acids and biomass burning derived organic species,

718 Environmental Science & Technology, 39, 1555-1562, 2005.

719 Chan, M. N., Kreidenweis, S. M., and Chan, C. K.: Measurements of the Hygroscopic and Deliquescence

720 Properties of Organic Compounds of Different Solubilities in Water and Their Relationship with Cloud

721 Condensation Nuclei Activities, Environmental Science & Technology, 42, 3602-3608, 2008.

722 Chan, M. N. C. a. C. K.: Mass transfer effects in hygroscopic measurements of aerosol particles,

723 Atmospheric Chemistry and Physics, 2005. 2005.

724 Cheung, H. H. Y., Yeung, M. C., Li, Y. J., Lee, B. P., and Chan, C. K.: Relative Humidity-Dependent

725 HTDMA Measurements of Ambient Aerosols at the HKUST Supersite in Hong Kong, China, Aerosol

726 Science and Technology, 49, 643-654, 2015.

727 Cheng, Y. F., Su, H., Rose, D., Gunthe, S. S., Berghof, M., Wehner, B., Achtert, P., Nowak, A., Takegawa,

728 N., Kondo, Y., Shiraiwa, M., Gong, Y. G., Shao, M., Hu, M., Zhu, T., Zhang, Y. H., Carmichael, G. R.,

729 Wiedensohler, A., Andreae, M. O., and Poschl, U.: Size-resolved measurement of the mixing state of soot

730 in the megacity Beijing, China: diurnal cycle, aging and parameterization, Atmospheric Chemistry and

731 Physics, 12, 4477-4491, 2012.

732 Choi, M. Y. and Chan, C. K.: The effects of organic species on the hygroscopic behaviors of inorganic

733 aerosols, Environmental science & technology, 36, 2422-2428, 2002.

734 Ciarelli, G., Aksoyoglu, S., Crippa, M., Jimenez, J. L., Nemitz, E., Sellegri, K., Äijälä, M., Carbone, S.,

735 Mohr, C., O'Dowd, C., Poulain, L., Baltensperger, U., and Prévôt, A. S. H.: Evaluation of European air

736 quality modelled by CAMx including the volatility basis set scheme, Atmos. Chem. Phys., 16, 10313-

737   10332, 2016.

738   Ciobanu, V. G., Marcolli, C., Krieger, U. K., Zuend, A., and Peter, T.: Efflorescence of ammonium sulfate

739   and coated ammonium sulfate particles: evidence for surface nucleation, The Journal of Physical

740   Chemistry A, 114, 9486-9495, 2010.

741   Clegg, S. L. and Seinfeld, J. H.: Thermodynamic models of aqueous solutions containing inorganic

742   electrolytes and dicarboxylic acids at 298.15 K. 2. Systems including dissociation equilibria, Journal of

743   Physical Chemistry A, 110, 5718-5734, 2006.

744   Clegg, S. L. and Wexler, A. S.: Densities and Apparent Molar Volumes of Atmospherically Important

745   Electrolyte Solutions. 1. The Solutes H2SO4, HNO3, HCl, Na2SO4, NaNO3, NaCl, (NH4)(2)SO4,

746   NH4NO3, and NH4Cl from 0 to 50 degrees C, Including Extrapolations to Very Low Temperature and

747   to the Pure Liquid State, and NaHSO4, NaOH, and NH3 at 25 degrees C, Journal of Physical Chemistry

748   A, 115, 3393-3460, 2011a.

749   Clegg, S. L. and Wexler, A. S.: Densities and apparent molar volumes of atmospherically important

750   electrolyte solutions. 2. The systems $H^{(+)}$-$HSO_4^{(-)}$-$SO_4^{(2-)}$-H_2O from 0 to 3 mol $kg^{(-1)}$ as a function of

751   temperature and $H^{(+)}$-$NH_4^{(+)}$-$HSO_4^{(-)}$-$SO_4^{(2-)}$-H_2O from 0 to 6 mol $kg^{(-1)}$ at 25 degrees C using a Pitzer ion

752   interaction model, and NH_4HSO_4-H_2O and $(NH_4)_3H(SO_4)_2$-H_2O over the entire concentration range, The

753   journal of physical chemistry. A, 115, 3461-3474, 2011b.

754   Decesari, S., Fuzzi, S., Facchini, M. C., Mircea, M., Emblico, L., Cavalli, F., Maenhaut, W., Chi, X.,

755   Schkolnik, G., Falkovich, A., Rudich, Y., Claeys, M., Pashynska, V., Vas, G., Kourtchev, I., Vermeylen,

756   R., Hoffer, A., Andreae, M. O., Tagliavini, E., Moretti, F., and Artaxo, P.: Characterization of the organic

757   composition of aerosols from Rondonia, Brazil, during the LBA-SMOCC 2002 experiment and its

758   representation through model compounds, Atmospheric Chemistry and Physics, 6, 375-402, 2006.

759   Denjean, C., Formenti, P., Picquet-Varrault, B., Pangui, E., Zapf, P., Katrib, Y., Giorio, C., Tapparo, A.,

760   Monod, A., and Temime-Roussel, B.: Relating hygroscopicity and optical properties to chemical

761   composition and structure of secondary organic aerosol particles generated from the ozonolysis of α-

762   pinene, Atmospheric Chemistry and Physics, 15, 3339-3358, 2015.

763   Dick, W. D., Saxena, P., and McMurry, P. H.: Estimation of water uptake by organic compounds in

764 submicron aerosols measured during the Southeastern Aerosol and Visibility Study, Journal of

765 Geophysical Research-Atmospheres, 105, 1471-1479, 2000.

766 Dusek, U., Frank, G. P., Massling, A., Zeromskiene, K., Iinuma, Y., Schmid, O., Helas, G., Hennig, T.,

767 Wiedensohler, A., and Andreae, M. O.: Water uptake by biomass burning aerosol at sub- and

768 supersaturated conditions: closure studies and implications for the role of organics, Atmospheric

769 Chemistry and Physics, 11, 9519-9532, 2011.

770 Engelhart, G. J., Hennigan, C. J., Miracolo, M. A., Robinson, A. L., and Pandis, S. N.: Cloud

771 condensation nuclei activity of fresh primary and aged biomass burning aerosol, Atmospheric Chemistry

772 and Physics, 12, 7285-7293, 2012.

773 Favez, O., Alfaro, S. C., Sciare, J., Cachier, H., and Abdelwahab, M. M.: Ambient measurements of light-

774 absorption by agricultural waste burning organic aerosols, Journal of Aerosol Science, 40, 613-620, 2009.

775 Feng, Y., Chen, Y., Guo, H., Zhi, G., Xiong, S., Li, J., Sheng, G., and Fu, J.: Characteristics of organic

776 and elemental carbon in PM2.5 samples in Shanghai, China, Atmospheric Research, 92, 434-442, 2009.

777 Frosch, M., Prisle, N. L., Bilde, M., Varga, Z., and Kiss, G.: Joint effect of organic acids and inorganic

778 salts on cloud droplet activation, Atmospheric Chemistry and Physics, 11, 3895-3911, 10.5194/acp-11-

779 3895-2011, 2011.

780 Gilman, J. B., Lerner, B. M., Kuster, W. C., Goldan, P. D., Warneke, C., Veres, P. R., Roberts, J. M., de

781 Gouw, J. A., Burling, I. R., and Yokelson, R. J.: Biomass burning emissions and potential air quality

782 impacts of volatile organic compounds and other trace gases from fuels common in the US, Atmos. Chem.

783 Phys., 15, 13915-13938, 2015.

784 Gupta, D., Eom, H. J., Cho, H. R., and Ro, C. U.: Hygroscopic behavior of NaCl–MgCl2 mixture

785 particles as nascent sea-spray aerosol surrogates and observation of efflorescence during humidification,

786 Atmos. Chem. Phys., 15, 11273-11290, 2015.

787 Hanford, K. L., Mitchem, L., Reid, J. P., Clegg, S. L., Topping, D. O., and McFiggans, G. B.:

788 Comparative thermodynamic studies of aqueous glutaric acid, ammonium sulfate and sodium chloride

789 aerosol at high humidity, Journal of Physical Chemistry A, 112, 9413-9422, 10.1021/jp802520d, 2008.

790 Hecobian, A., Zhang, X., Zheng, M., Frank, N., Edgerton, E. S., and Weber, R. J.: Water-Soluble Organic
791 Aerosol material and the light-absorption characteristics of aqueous extracts measured over the
792 Southeastern United States, Atmospheric Chemistry and Physics, 10, 5965-5977, 2010.

793 Hegg, D. A., Warren, S. G., Grenfell, T. C., Doherty, S. J., and Clarke, A. D.: Sources of light-absorbing
794 aerosol in arctic snow and their seasonal variation, Atmospheric Chemistry and Physics, 10, 10923-10938,
795 2010.

796 Hodas, N., Zuend, A., Mui, W., Flagan, R., and Seinfeld, J.: Influence of particle-phase state on the
797 hygroscopic behavior of mixed organic–inorganic aerosols, Atmospheric Chemistry and Physics, 15,
798 5027-5045, 2015.

799 Hodas, N., Zuend, A., Schilling, K., Berkemeier, T., Shiraiwa, M., Flagan, R. C., and Seinfeld, J. H.:
800 Discontinuities in hygroscopic growth below and above water saturation for laboratory surrogates of
801 oligomers in organic atmospheric aerosols, Atmos. Chem. Phys., doi: 10.5194/acp-16-12767-2016, 2016.

802 Jacobson, M. Z.: Effects of biomass burning on climate, accounting for heat and moisture fluxes, black
803 and brown carbon, and cloud absorption effects, Journal of Geophysical Research-Atmospheres, 119,
804 8980-9002, 2014.

805 Jedelsk´y Jiri, L. ı. H. e. y., Pavel Hynˇcica, and Ivan and Cibulka: Partial molar volumes of organic
806 solutes in water. IV. Benzoic and hydroxybenzoic acids at temperatures from T D 298 K to T D 498 K
807 and pressures up to 30 MPa, J. Chem. Thermodynamics, 32, 11, 2000.

808 Jing, B., Tong, S., Liu, Q., Li, K., Wang, W., Zhang, Y., and Ge, M.: Hygroscopic behavior of
809 multicomponent organic aerosols and their internal mixtures with ammonium sulfate, Atmospheric
810 Chemistry and Physics, 16, 4101-4118, 2016.

811 Kim, J., Ahlm, L., Yli-Juuti, T., Lawler, M., Keskinen, H., Tröstl, J., Schobesberger, S., Duplissy, J.,
812 Amorim, A., Bianchi, F., Donahue, N. M., Flagan, R. C., Hakala, J., Heinritzi, M., Jokinen, T., Kürten,
813 A., Laaksonen, A., Lehtipalo, K., Miettinen, P., Petäjä, T., Rissanen, M. P., Rondo, L., Sengupta, K.,
814 Simon, M., Tomé, A., Williamson, C., Wimmer, D., Winkler, P. M., Ehrhart, S., Ye, P., Kirkby, J., Curtius,
815 J., Baltensperger, U., Kulmala, M., Lehtinen, K. E. J., Smith, J. N., Riipinen, I., and Virtanen, A.:
816 Hygroscopicity of nanoparticles produced from homogeneous nucleation in the CLOUD experiments,

817   Atmos. Chem. Phys., 16, 293-304, 2016.

818   Kiss, G., Tombácz, E., and Hansson, H.-C.: Surface Tension Effects of Humic-Like Substances in the

819   Aqueous Extract of Tropospheric Fine Aerosol, Journal of Atmospheric Chemistry, 50, 279-294, 2005.

820   Koop, T., Bookhold, J., Shiraiwa, M., and Poschl, U.: Glass transition and phase state of organic

821   compounds: dependency on molecular properties and implications for secondary organic aerosols in the

822   atmosphere, Physical Chemistry Chemical Physics, 13, 19238-19255, 2011.

823   Konovalov, I. B., Beekmann, M., Berezin, E. V., Petetin, H., Mielonen, T., Kuznetsova, I. N., and Andreae,

824   M. O.: The role of semi-volatile organic compounds in the mesoscale evolution of biomass burning

825   aerosol: a modeling case study of the 2010 mega-fire event in Russia, Atmos. Chem. Phys., 15, 13269-

826   13297, 2015.

827   Laborde, M., Crippa, M., Tritscher, T., Juranyi, Z., Decarlo, P. F., Temime-Roussel, B., Marchand, N.,

828   Eckhardt, S., Stohl, A., Baltensperger, U., Prevot, A. S. H., Weingartner, E., and Gysel, M.: Black carbon

829   physical properties and mixing state in the European megacity Paris, Atmospheric Chemistry and Physics,

830   13, 5831-5856, 2013.

831   Lack, D. A., Bahreni, R., Langridge, J. M., Gilman, J. B., and Middlebrook, A. M.: Brown carbon

832   absorption linked to organic mass tracers in biomass burning particles, Atmospheric Chemistry and

833   Physics, 13, 2415-2422, 2013.

834   Lack, D. A., Bahreni, R., Langridge, J. M., Gilman, J. B., and Middlebrook, A. M.: Brown carbon

835   absorption linked to organic mass tracers in biomass burning particles, Atmospheric Chemistry and

836   Physics, 13, 2415-2422, 2013.

837   Lack, D. A., Langridge, J. M., Bahreini, R., Cappa, C. D., Middlebrook, A. M., and Schwarz, J. P.: Brown

838   carbon and internal mixing in biomass burning particles, Proceedings of the National Academy of

839   Sciences of the United States of America, 109, 14802-14807, 2012.

840   Lawson, S. J., Keywood, M. D., Galbally, I. E., Gras, J. L., Cainey, J. M., Cope, M. E., Krummel, P. B.,

841   Fraser, P. J., Steele, L. P., Bentley, S. T., Meyer, C. P., Ristovski, Z., and Goldstein, A. H.: Biomass

842   burning emissions of trace gases and particles in marine air at Cape Grim, Tasmania, Atmos. Chem. Phys.,

843   15, 13393-13411, 2015.

844   Lee, Y. N.: Airborne measurement of inorganic ionic components of fine aerosol particles using the

845   particle-into-liquid sampler coupled to ion chromatography technique during ACE-Asia and TRACE-P,

846   Journal of Geophysical Research, doi:10.1029/2002JD003265, 2003.

847   Lei, T., Zuend, A., Wang, W. G., Zhang, Y. H., and Ge, M. F.: Hygroscopicity of organic compounds from

848   biomass burning and their influence on the water uptake of mixed organic ammonium sulfate aerosols,

849   Atmospheric Chemistry and Physics, 14, 1-20, 2014.

850   Lienhard, D. M., Bones, D. L., Zuend, A., Krieger, U. K., Reid, J. P., and Peter, T.: Measurements of

851   thermodynamic and optical properties of selected aqueous organic and organic-inorganic mixtures of

852   atmospheric relevance, The journal of physical chemistry. A, 116, 9954-9968, 2012.

853   Liu, B. Y. H., Pui, D. Y. H., and Rubow, K. L. a. S., W.W.: ELECTROSTATIC EFFECTS IN AEROSOL

854   SAMPLING AND FILTRATION, Arm. occup. Hyg., 29, 251-269, 1985.

855   Liu, J. M., Scheuer, E., Dibb, J., Ziemba, L. D., Thornhill, K. L., Anderson, B. E., Wisthaler, A., Mikoviny,

856   T., Devi, J. J., Bergin, M., and Weber, R. J.: Brown carbon in the continental troposphere, Geophysical

857   Research Letters, 41, 2191-2195, 2014.

858   Liu, Q., Jing, B., Peng, C., Tong, S., Wang, W., and Ge, M.: Hygroscopicity of internally mixed multi-

859   component aerosol particles of atmospheric relevance, Atmos. Environ., 125, 69-77, 2016.

860   Malm, W. C. and Kreidenweis, S. M.: The effects of models of aerosol hygroscopicity on the

861   apportionment of extinction, Atmos. Environ., 31, 1965-1976, 1997.

862   MAN NIN CHAN, A. K. Y. L., AND and CHAN, C. K.: Responses of Ammonium Sulfate Particles

863   Coated with Glutaric Acid to Cyclic Changes in Relative Humidity: Hygroscopicity and Raman

864   Characterization, Environ.Sci.Technol., 40, 6893-6989, 2006.

865   Man Nin Chan, C. K. C.: Mass transfer effects on the hygroscopic growth of ammonium sulfate particles

866   with a water-insoluble coating, Atmos. Environ., doi: 10.1016/j.atmosenv.2007.01.047, 2007.

867   Marcolli, C. and Peter, T.: Water activity in polyol/water systems: new UNIFAC parameterization, Atmos.

868   Chem. Phys., 5, 1545-1555, 2005.

869   Marshall, F. H., Miles, R. E. H., Song, Y.-C., Ohm, P. B., Power, R. M., Reid, J. P., and Dutcher, C. S.:

870   Diffusion and reactivity in ultraviscous aerosol and the correlation with particle viscosity, Chemical

871   Science, 7, 1298-1308, 2016.

872   Martin, M., Tritscher, T., Juranyi, Z., Heringa, M. F., Sierau, B., Weingartner, E., Chirico, R., Gysel, M.,

873   Prevot, A. S. H., Baltensperger, U., and Lohmann, U.: Hygroscopic properties of fresh and aged wood

874   burning particles, Journal of Aerosol Science, 56, 15-29, 2013.

875   Mikhailov, E., Vlasenko, S., Rose, D., and Pöschl, U.: Mass-based hygroscopicity parameter interaction

876   model and measurement of atmospheric aerosol water uptake, Atmospheric Chemistry and Physics, 13,

877   717-740, 2013.

878   Mochida, M. and Kawamura, K.: Hygroscopic properties of levoglucosan and related organic compounds

879   characteristic to biomass burning aerosol particles, Journal of Geophysical Research-Atmospheres,

880   doi:10.1029/2004JD004962, 2004.

881   Moosmuller, H., Chakrabarty, R. K., and Arnott, W. P.: Aerosol light absorption and its measurement: A

882   review, Journal of Quantitative Spectroscopy & Radiative Transfer, 110, 844-878, 2009.

883   Paglione, M., Saarikoski, S., Carbone, S., Hillamo, R., Facchini, M. C., Finessi, E., Giulianelli, L.,

884   Carbone, C., Fuzzi, S., Moretti, F., Tagliavini, E., Swietlicki, E., Stenstrom, K. E., Prevot, A. S. H.,

885   Massoli, P., Canaragatna, M., Worsnop, D., and Decesari, S.: Primary and secondary biomass burning

886   aerosols determined by proton nuclear magnetic resonance (H-1-NMR) spectroscopy during the 2008

887   EUCAARI campaign in the Po Valley (Italy), Atmospheric Chemistry and Physics, 14, 5089-5110, 2014.

888   Pajunoja, A, AT Lambe, J Hakala, N Rastak, MJ Cummings, JF Brogan, L Hao, M Paramonov, J

889   Hong, NL Prisle, J Malila, S Romakkaniemi, KEJ Lehtinen, A Laaksonen, M Kulmala, P Massoli, TB

890   Onasch, NM   Donahue, I   Riipinen, P   Davidovits, DR   Worsnop, T   Petäjä,   and A

891   Virtanen (2015), Adsorptive uptake of water by semisolid secondary organic aerosols. Geophys. Res.

892   Lett., 42, 3063–3068. doi: 10.1002/2015GL063142.

893   Ovadnevaite, J., Zuend, A., Laaksonen, A., Sanchez, K. J., Roberts, G., Ceburnis, D., Decesari, S.,

894 Rinaldi, M., Hodas, N., Facchini, M. C., Seinfeld, J. H., and O' Dowd, C.: Surface tension prevails over

895 solute effect in organic-influenced cloud droplet activation, Nature, 546, 637-641, 10.1038/nature22806,

896 2017.

897 Peng, C., Chan, M. N., and Chan, C. K.: The hygroscopic properties of dicarboxylic and multifunctional

898 acids: Measurements and UNIFAC predictions, Environmental Science & Technology, 35, 4495-4501,

899 2001.

900 Petters, M. D. and. Kreidenweis, S. M.: A single parameter representation of hygroscopic growth and

901 cloud condensation nucleus activity, Atmos. Chem. Phys., 7, 1961-1971, 2007.

902 Pöhlker, M. L., Pöhlker, C., Ditas, F., Klimach, T., Hrabe de Angelis, I., Araújo, A., Brito, J., Carbone,

903 S., Cheng, Y., and Chi, X.: Long-term observations of cloud condensation nuclei in the Amazon rain

904 forest–Part 1: Aerosol size distribution, hygroscopicity, and new model parametrizations for CCN

905 prediction, Atmospheric Chemistry and Physics, 16, 15709-15740, 2016.

906 Powelson, M. H., Espelien, B. M., Hawkins, L. N., Galloway, M. M., and De Haan, D. O.: Brown Carbon

907 Formation by Aqueous-Phase Carbonyl Compound Reactions with Amines and Ammonium Sulfate,

908 Environmental Science & Technology, 48, 985-993, 2014.

909 Pratt, K. A., Murphy, S. M., Subramanian, R., DeMott, P. J., Kok, G. L., Campos, T., Rogers, D. C.,

910 Prenni, A. J., Heymsfield, A. J., Seinfeld, J. H., and Prather, K. A.: Flight-based chemical characterization

911 of biomass burning aerosols within two prescribed burn smoke plumes, Atmospheric Chemistry and

912 Physics, 11, 12549-12565, 2011.

913 Pratt, K. A. and Prather, K. A.: Aircraft measurements of vertical profiles of aerosol mixing states, Journal

914 of Geophysical Research, doi:10.1029/2009JD013150, 2010.

915 Rastak, N., Pajunoja, A., Acosta Navarro, J. C., Ma, J., Song, M., Partridge, D. G., Kirkevåg, A., Leong,

916 Y., Hu, W. W., Taylor, N. F., Lambe, A., Cerully, K., Bougiatioti, A., Liu, P., Krejci, R., Petäjä, T., Percival,

917 C., Davidovits, P., Worsnop, D. R., Ekman, A. M. L., Nenes, A., Martin, S., Jimenez, J. L., Collins, D.

918 R., Topping, D. O., Bertram, A. K., Zuend, A., Virtanen, A., and Riipinen, I.: Microphysical explanation

919 of the RH-dependent water affinity of biogenic organic aerosol and its importance for climate,

920 Geophysical Research Letters, doi: 10.1002/2017GL073056. 2017.

921 Reid, J. P., Dennis-Smither, B. J., Kwamena, N.-O. A., Miles, R. E. H., Hanford, K. L., and Homer, C.

922 J.: The morphology of aerosol particles consisting of hydrophobic and hydrophilic phases: hydrocarbons,

923 alcohols and fatty acids as the hydrophobic component, Physical Chemistry Chemical Physics, 13,

924 15559-15572, 2011.

925 Renbaum-Wolff, L., Song, M., Marcolli, C., Zhang, Y., Liu, P. F., Grayson, J. W., Geiger, F. M., Martin,

926 S. T., and Bertram, A. K.: Observations and implications of liquid–liquid phase separation at high relative

927 humidities in secondary organic material produced by α-pinene ozonolysis without inorganic salts,

928 Atmos. Chem. Phys., 16, 7969-7979, 2016.

929 Rissler, J., Vestin, A., Swietlicki, E., Fisch, G., Zhou, J., Artaxo, P., and Andreae, M. O.: Size distribution

930 and hygroscopic properties of aerosol particles from dry-season biomass burning in Amazonia,

931 Atmospheric Chemistry and Physics, 6, 471-491, 2006.

932 Rizzo, L. V., Correia, A. L., Artaxo, P., Procopio, A. S., and Andreae, M. O.: Spectral dependence of

933 aerosol light absorption over the Amazon Basin, Atmospheric Chemistry and Physics, 11, 8899-8912,

934 2011.

935 Rose, D., Gunthe, S. S., Su, H., Garland, R. M., Yang, H., Berghof, M., Cheng, Y. F., Wehner, B., Achtert,

936 P., Nowak, A., Wiedensohler, A., Takegawa, N., Kondo, Y., Hu, M., Zhang, Y., Andreae, M. O., and

937 Poschl, U.: Cloud condensation nuclei in polluted air and biomass burning smoke near the mega-city

938 Guangzhou, China -Part 2: Size-resolved aerosol chemical composition, diurnal cycles, and externally

939 mixed weakly CCN-active soot particles, Atmospheric Chemistry and Physics, 11, 2817-2836, 2011.

940 Saarnio, K., Aurela, M., Timonen, H., Saarikoski, S., Teinila, K., Makela, T., Sofiev, M., Koskinen, J.,

941 Aalto, P. P., Kulmala, M., Kukkonen, J., and Hillamo, R.: Chemical composition of fine particles in fresh

942 smoke plumes from boreal wild-land fires in Europe, Science of the Total Environment, 408, 2527-2542,

943 2010.

944 Sadezky, A., Muckenhuber, H., Grothe, H., Niessner, R., and Poschl, U.: Raman micro spectroscopy of

945 soot and related carbonaceous materials: Spectral analysis and structural information, Carbon, 43, 1731-

946 1742, 2005.

947 Saleh, R., Hennigan, C. J., McMeeking, G. R., Chuang, W. K., Robinson, E. S., Coe, H., Donahue, N.

948 M., and Robinson, A. L.: Absorptivity of brown carbon in fresh and photo-chemically aged biomass-

949 burning emissions, Atmospheric Chemistry and Physics, 13, 7683-7693, 2013.

950 Saleh, R., Robinson, E. S., Tkacik, D. S., Ahern, A. T., Liu, S., Aiken, A. C., Sullivan, R. C., Presto, A.

951 A., Dubey, M. K., Yokelson, R. J., Donahue, N. M., and Robinson, A. L.: Brownness of organics in

952 aerosols from biomass burning linked to their black carbon content, Nature Geoscience, 7, 647-650, 2014.

953 Seinfeld, J. and Pandis, S.: Atmospheric chemistry and physics. Hoboken. NJ: Wiley, 2006.

954 Shantanu H. Jathar, A. M., Kekkey C. Barsabti, William E. Asher, James F, Pankow and Michael J.

955 Kleeman: Water uptake by organic aerosol and its influence on gas/particle partitioning of secondary

956 organic aerosol in the United States doi: 10.1016/j.atmosenv.2016.01.001, 2016.

957 Shiraiwa, M., Zuend, A., Bertram, A. K., and Seinfeld, J. H.: Gas-particle partitioning of atmospheric

958 aerosols: interplay of physical state, non-ideal mixing and morphology, Physical Chemistry Chemical

959 Physics, 15, 11441-11453, 2013.

960 Sjogren, S., Gysel, M., Weingartner, E., Baltensperger, U., Cubison, M. J., Coe, H., Zardini, A. A.,

961 Marcolli, C., Krieger, U. K., and Peter, T.: Hygroscopic growth and water uptake kinetics of two-phase

962 aerosol particles consisting of ammonium sulfate, adipic and humic acid mixtures, Journal of Aerosol

963 Science, 38, 157-171, 2007.

964 Smith, M. L., Bertram, A. K., and Martin, S. T.: Deliquescence, efflorescence, and phase miscibility of

965 mixed particles of ammonium sulfate and isoprene-derived secondary organic material, Atmospheric

966 Chemistry and Physics, 12, 9613-9628, 2012.

967 Song, M., Marcolli, C., Krieger, U. K., Zuend, A., and Peter, T.: Liquid-liquid phase separation and

968 morphology of internally mixed dicarboxylic acids/ammonium sulfate/water particles, Atmospheric

969 Chemistry and Physics, 12, 2691-2712, 2012.

970 Song, M., Marcolli, C., Krieger, U. K., Zuend, A., and Peter, T.: Liquid-liquid phase separation in aerosol

971 particles: Dependence on O:C, organic functionalities, and compositional complexity, Geophysical

972 Research Letters, 39, doi:10.1029/2012GL052807, 2012.

973 Srinivas, B. and Sarin, M. M.: Brown carbon in atmospheric outflow from the Indo-Gangetic Plain: Mass

974   absorption efficiency and temporal variability, Atmos. Environ., 89, 835-843, 2014.

975   Srinivas, B. and Sarin, M. M.: Light absorbing organic aerosols (brown carbon) over the tropical Indian

976   Ocean: impact of biomass burning emissions, Environmental Research Letters, doi:10.1088/1748-

977   9326/8/4/044042, 2013.

978   Svenningsson, B., Rissler, J., Swietlicki, E., Mircea, M., Bilde, M., Facchini, M. C., Decesari, S., Fuzzi,

979   S., Zhou, J., Monster, J., and Rosenorn, T.: Hygroscopic growth and critical supersaturations for mixed

980   aerosol particles of inorganic and organic compounds of atmospheric relevance, Atmospheric Chemistry

981   and Physics, 6, 1937-1952, 2006.

982   Topping, D., McFiggans, G., and Coe, H.: A curved multi-component aerosol hygroscopicity model

983   framework: Part 1–Inorganic compounds, Atmospheric Chemistry and Physics, 5, 1205-1222, 2005.

984   Tuckermann, R. a. C., H. K.: The surface tension of aqueous solutions of some atmospheric water-soluble

985   organic compounds, Atmos. Environ., 38, 6135-6138, 2004.

986   Väkevä, M., Kulmala, M., Stratmann, F., and Hämeri, K.: Field measurements of hygroscopic properties

987   and state of mixing of nucleation mode particles, Atmospheric Chemistry and Physics, 2, 55-66, 2002.

988   Veghte, D. P., Altaf, M. B., and Freedman, M. A.: Size dependence of the structure of organic aerosol,

989   Journal of the American Chemical Society, 135, 16046-16049, 2013.

990   Gonçalves, W. A., Machado, L. A. T., and Kirstetter, P.-E.: Influence of biomass aerosol on precipitation

991   over the Central Amazon: an observational study, Atmos. Chem. Phys., doi: 10.5194/acp-15-6789-2015,

992   2015.

993   Wang, J., Cubison, M. J., Aiken, A. C., Jimenez, J. L., and Collins, D. R.: The importance of aerosol

994   mixing state and size-resolved composition on CCN concentration and the variation of the importance

995   with atmospheric aging of aerosols, Atmospheric Chemistry and Physics, 10, 7267-7283, 2010.

996   Wang, X., Heald, C. L., Ridley, D. A., Schwarz, J. P., Spackman, J. R., Perring, A. E., Coe, H., Liu, D.,

997   and Clarke, A. D.: Exploiting simultaneous observational constraints on mass and absorption to estimate

998   the global direct radiative forcing of black carbon and brown carbon, Atmospheric Chemistry and Physics,

999   14, 10989-11010, 2014.

Whitehead, J. D., Darbyshire, E., Brito, J., Barbosa, H. M., Crawford, I., Stern, R., Gallagher, M. W., Kaye, P. H., Allan, J. D., and Coe, H.: Biogenic cloud nuclei in the central Amazon during the transition from wet to dry season, Atmospheric Chemistry and Physics, 16, 9727-9743, 2016.

Wu, Z. J., Zheng, J., Shang, D. J., Du, Z. F., Wu, Y. S., Zeng, L. M., Wiedensohler, A., and Hu, M.: Particle hygroscopicity and its link to chemical composition in the urban atmosphere of Beijing, China, during summertime, Atmos. Chem. Phys., 16, 1123-1138, 2016.

Yates III, L. M., Wandruszka, R.V.: Decontamination of polluted water bytreatment with a crude humic acid blend, Environmental Science and Technology, 33, 2076-2080, 1999.

You, Y. and Bertram, A. K.: Effects of molecular weight and temperature on liquid–liquid phase separation in particles containing organic species and inorganic salts, Atmospheric Chemistry and Physics, 15, 1351-1365, 2015.

You, Y., Renbaum-Wolff, L., and Bertram, A. K.: Liquid–liquid phase separation in particles containing organics mixed with ammonium sulfate, ammonium bisulfate, ammonium nitrate or sodium chloride, Atmospheric Chemistry and Physics, 13, 11723-11734, 2013.

Yuan Youa, L. R.-W., Marc Carreras-Sospedrab, Sarah J. Hannaa, Naruki Hiranumac, Saeid Kamald,, Mackenzie L. Smithe, X. Z., Rodney J. Weberf, John E. Shillingg, Donald Dabdubb, Scot T. Martine,h,1,, and Bertrama, a. A. K.: Images reveal that atmospheric particles can undergo liquid–liquid phase separations, pnas, 109, 13188-13193, 2012.

Zamora, I. R., Tabazadeh, A., Golden, D. M., and Jacobson, M. Z.: Hygroscopic growth of common organic aerosol solutes, including humic substances, as derived from water activity measurements, Journal of Geophysical Research: Atmospheres, doi:10.1029/2011JD016067, 2011.

Zardini, A. A., Sjogren, S., Marcolli, C., Krieger, U. K., Gysel, M., Weingartner, E., Baltensperger, U., and Peter, T.: A combined particle trap/HTDMA hygroscopicity study of mixed inorganic/organic aerosol particles, Atmospheric Chemistry and Physics, 8, 5589-5601, 2008.

Zawadowicz, M., Proud, S., Seppalainen, S., and Cziczo, D.: Hygroscopic and phase separation properties of ammonium sulfate/organics/water ternary solutions, Atmospheric Chemistry and Physics,

1026   15, 8975-8986, 2015.

1027   Zhang, Q., Jimenez, J. L., Canagaratna, M. R., Allan, J. D., Coe, H., Ulbrich, I., Alfarra, M. R., Takami,

1028   A., Middlebrook, A. M., Sun, Y. L., Dzepina, K., Dunlea, E., Docherty, K., DeCarlo, P. F., Salcedo, D.,

1029   Onasch, T., Jayne, J. T., Miyoshi, T., Shimono, A., Hatakeyama, S., Takegawa, N., Kondo, Y., Schneider,

1030   J., Drewnick, F., Borrmann, S., Weimer, S., Demerjian, K., Williams, P., Bower, K., Bahreini, R., Cottrell,

1031   L., Griffin, R. J., Rautiainen, J., Sun, J. Y., Zhang, Y. M., and Worsnop, D. R.: Ubiquity and dominance

1032   of oxygenated species in organic aerosols in anthropogenically-influenced Northern Hemisphere

1033   midlatitudes, Geophysical Research Letters, doi:10.1029/2007GL029979, 2007.

1034   Zhang, S. L., Ma, N., Kecorius, S., Wang, P. C., Hu, M., Wang, Z. B., Größ, J., Wu, Z. J., and

1035   Wiedensohler, A.: Mixing state of atmospheric particles over the North China Plain, Atmos. Environ.,

1036   125, Part A, 152-164, 2016.

1037   Zhong, M. and Jang, M.: Dynamic light absorption of biomass-burning organic carbon photochemically

1038   aged under natural sunlight, Atmospheric Chemistry and Physics, 14, 1517-1525, 2014.

1039   Zuend, A., Marcolli, C., Booth, A. M., Lienhard, D. M., Soonsin, V., Krieger, U. K., Topping, D. O.,

1040   McFiggans, G., Peter, T., and Seinfeld, J. H.: New and extended parameterization of the thermodynamic

1041   model AIOMFAC: calculation of activity coefficients for organic-inorganic mixtures containing carboxyl,

1042   hydroxyl, carbonyl, ether, ester, alkenyl, alkyl, and aromatic functional groups, Atmospheric Chemistry

1043   and Physics, 11, 9155-9206, 2011.

1044   Zuend, A., Marcolli, C., Luo, B. P., and Peter, T.: A thermodynamic model of mixed organic-inorganic

1045   aerosols to predict activity coefficients, Atmospheric Chemistry and Physics, 8, 4559-4593, 2008.

1046   Zuend, A., Marcolli, C., Peter, T., and Seinfeld, J. H.: Computation of liquid-liquid equilibria and phase

1047   stabilities: implications for RH-dependent gas/particle partitioning of organic-inorganic aerosols,

1048   Atmospheric Chemistry and Physics, 10, 7795-7820, 2010.

1049   Zuend, A. and Seinfeld, J. H.: Modeling the gas-particle partitioning of secondary organic aerosol: the

1050   importance of liquid-liquid phase separation, Atmospheric Chemistry and Physics, 12, 3857-3882, 2012.

1051

1052 **Table 1.** Substances and their physical properties used in this work.

Chemical compound	Chemical formula	Molar Mass [g mol^{-1}]	Density in solid or liquid state [g cm^{-3}]	Solubility g/100cm^3 H$_2$O	Solution surface tension [J m^{-2}]	Manufacturer
Ammonium sulfate	$(NH_4)_2SO_4$	132.140	1.770[a] (solid), 1.550[a](liquid)	74.400(at 20℃)	0.072(0.001-10mg/mL)	Alfa Aesar, 99.95%
Levoglucosan	$C_6H_{10}O_5$	126.100	1.618[b](solid) 1.512[b](liquid)		0.073[e] (0.01-10mg/mL)	Aldrich, 99%
4-Hydroxybenzoic acid	$C_7H_6O_3$	138.100	1.460(solid) 1.372[f](liquid)	0.675(at 25℃)	0.070[g] (>10mg/mL)	Alfa Aesar, 99.99%
Humic acid		NA	0.800[h](solid)	NA	NA	Aldrich, 99%

1053 [a]Clegg and Wexler, (2011);
1054 [b]Lienhard et al, (2012);
1055 [e]Tuckermann and Cammenga (2004) at 293K;
1056 [f]Jedelsky et al, (2000);
1057 [g]Kiss et al, (2005);
1058 [h]Yates III and Wandruszka, (1999);

1059

1060

1061

1062

1063

1064

1065

1066

1067

1068

1069

1070   **Table 2.** The chemical composition of biomass-burning model mixtures studied given as mass
1071   percentages (wt %).

Mixture name	Levoglucosan	4-Hydroxybenzoic acid	Humic acid	Ammonium sulfate
Mix-bio-dry	87.2%	9.2%	1.5%	2.1%
Mix-bio-wet	68.0%	26.0%	3.0%	3.0%

1072

1073

1074

1075

1076

1077

1078

1079

1080

1081

1082

1083

1084

1085

1086

1087

1088

1089

1090   **Table 3.** Coefficients (c_1, c_2, c_3) of the fitted growth factor parameterization (Eq. 5) as follows:

Chemical compounds	c_1	c_2	c_3
Levoglucosan	0.12868746	0.36582023	-0.39840382
4-Hydroxybenzoic acid	-1.389967E-01	2.325586E-01	-9.891943E-02
Humic acid	-1.618304E-02	2.202483E-01	2.005134E-02

1091

1092

1093

1094

1095

1096

1097

1098

1099

1100

1101

1102

1103

1104

1105

1106

1107

1108 **Table 4:** Experimental studies of organic and ammonium sulfate (AS) deliquescence and efflorescence
1109 RH from this work and previous studies at 298K.

Signal compound/Mixture	Organic mass fraction (%)	Deliquescence relative humidity of AS or organic in the mixed particle	Efflorescence relative humidity of AS or organic in the mixed particle
Levoglucosan	-	80%[a]*	< 4%[a]*
		82.8%[b]	
	25	80%	45%
Levoglucosan+AS	50	-	-
	75	-	-
4-hygroxybenzoic acid	-	> 97%[a]*	< 4%[a]*
	25	80%	35%
4-Hydroxybenzoic acid+AS	50	80%	25%
	75	80%	-
Humic acid	-	-	-
	20	80%	35%
Humic acid+AS	50	80%	35%
	75	80%	35%

1110 *is the DRH and ERH of pure organic components.

1111 [a]Mochida and Kawamura. (2004)

1112 [b]Zamora et al. (2011)

1113

1114

1115

1116

1117
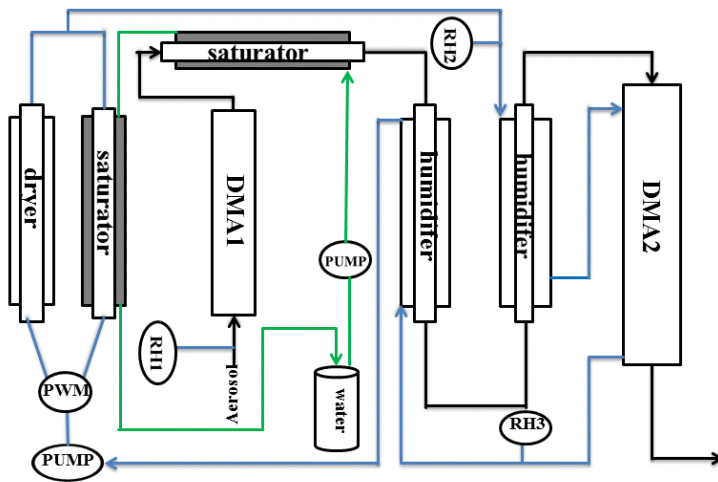
1118

1119 **Figure 1.** Schematic of the hygroscopicity tandem different mobility analyzer (HTDMA) system. the

1120 sheath flow, aerosol flow, and water flow have been represented by the blue, black, green line,

1121 respectively. PWM: Pulse Width Modulator circuit.

1122

1123

1124

1125

1126

1127
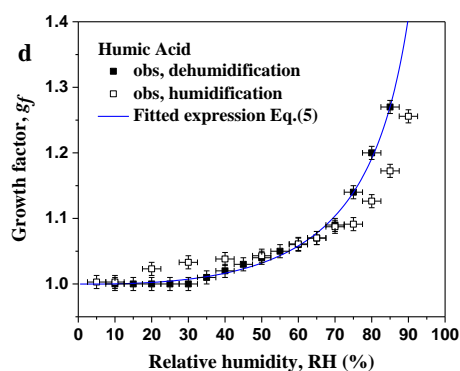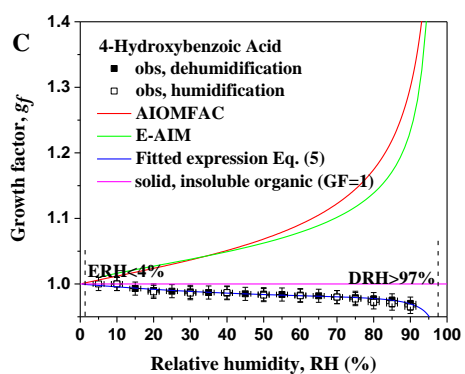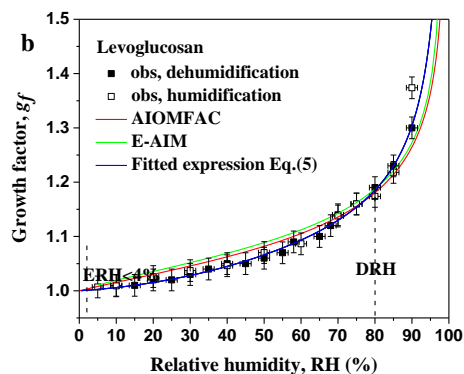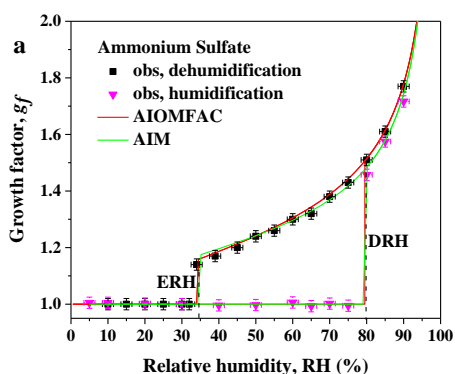
1128

1129

1130 **Figure 2.** Hygroscopic growth, deliquescence and efflorescence of aerosol particles. Hygroscopic growth

1131 factors of (**a**) ammonium sulfate (AS), (**b**) levoglucosan, (**c**) 4-hydroxybenzoic acid, and (**d**) humic acid

1132 aerosol particles with dry diameter of 100 nm (open, black square). In this study, the green curves show

1133 E-AIM predictions, and the red curves the AIOMFAC predictions, and the blue lines the fitted expression

1134 (Eq. 5).

1135

1136

1137
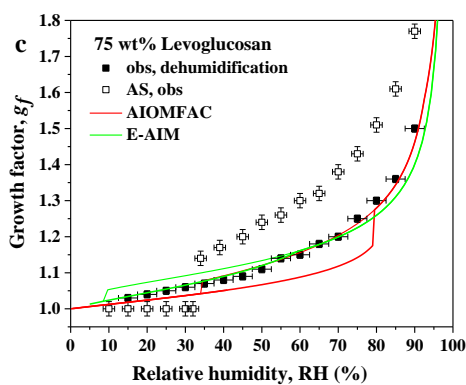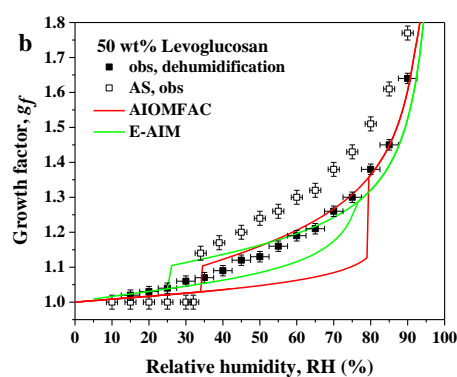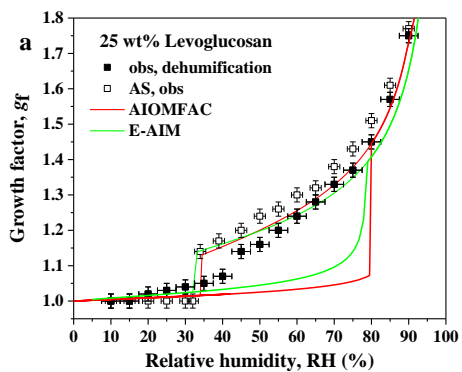
1138

1139

1140 **Figure 3.** Hygroscopic growth, efflorescence of aerosol particles, and model predictions represent the

1141 diameter growth factor during dehydration experiments in the range from 90 % to 5 % RH at 298.15 K.

1142 (**a,b,c**). Hygroscopic growth curves of mixtures consisting of levoglucosan and ammonium sulfate (solid

1143 symbols) at three different dry state mass fraction for particles of an initial dry diameter of 100 nm at RH

1144 < 5 %) as compared to that of pure ammonium sulfate (open symbols, "AS, obs"). AIOMFAC-based

1145 model predictions for bulk systems are shown in red, E-AIM predictions are shown in green.

1146

1147
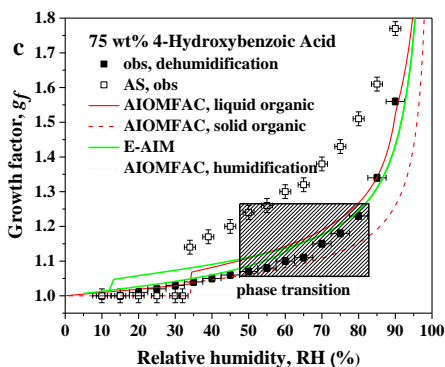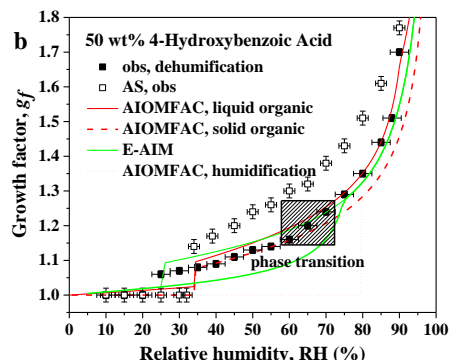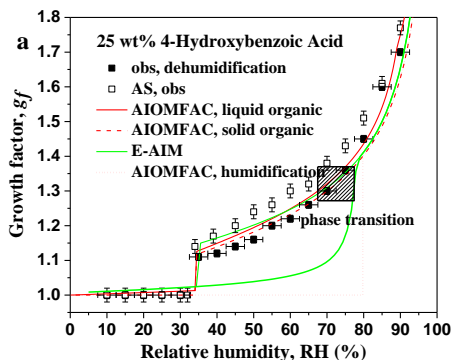
1148

1149

Figure 4. Hygroscopic growth factors, efflorescence of behavior, and model predications for dehydration experiments in the range from 90 % to 5 % RH at 298.15 K. (**a,b,c**) hygroscopic growth curves of mixtures consisting of 4-hydroxybenzoic acid and ammonium sulfate (solid symbols) at three different dry state mass fraction (initial dry diameter of 100 nm at RH < 5 %) as compared to that of pure ammonium sulfate (open symbols). AIOMFAC-based model predictions for bulk systems are shown in red, E-AIM-predictions are shown in green for the case of assuming that 4-hydroxybenzoic acid remains in the liquid state. Shaded rectangle: RH range of gradual crystallization of 4-hydroxybenzoic acid.

1157
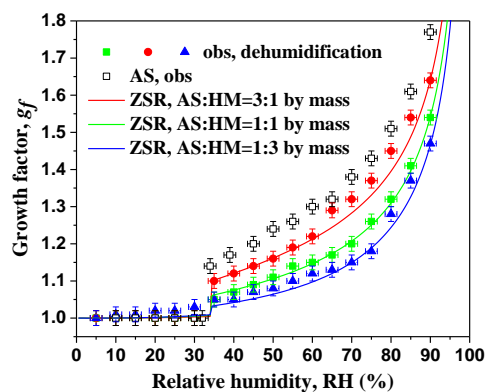
1158

Figure 5. Hygroscopic growth factors, efflorescence of aerosol particles/constituents consisting of humic acid and ammonium sulfate at three different dry state mass fractions with initial dry diameter of 100 nm at RH < 5 % as compared to that of pure ammonium sulfate (open symbols). Colored curves: ZSR predictions of dimeter growth factors for dry particle compositions corresponding to the experimental data during dehumidification in the range from 90 % to 5 % RH at 298.15 K.
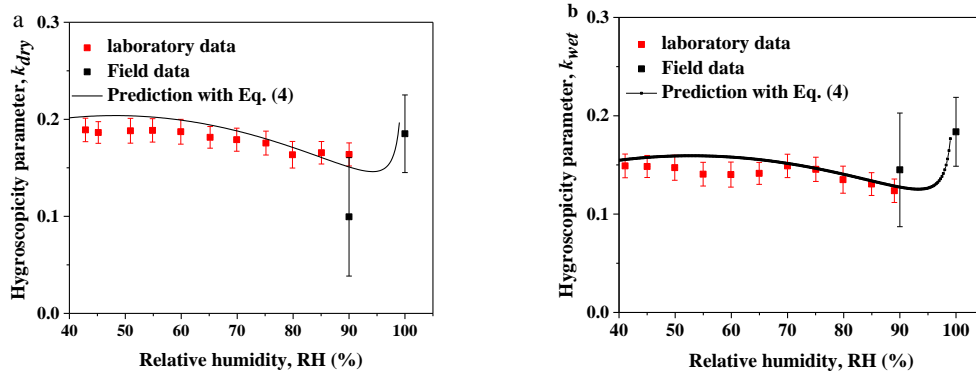
1159

1160

1161

1162

1163

1164

1165

1166

1167

1168

1169

1170

1171

1172

1173

1174

1175

Figure 6. Hygroscopicity parameter, κ, representing mixed aerosol particles consisting of organic

surrogate components and ammonium sulfate at different periods (initial dry diameter of 100 nm at RH

< 5 %). The black curves in panels (a, b) show the κ prediction from Eq. (4) with HGF_{mix} calculated by

Eq. (6) using component volume fractions and the HGF of the individual mixture components from a fit

to the laboratory data (using Eq.5). the black symbols and error bars show field data from the Amazon

during the dry and wet periods at conditions of water vapor sub-saturation (HTDMA measurement) and

super-saturation (κ_{CNN}) (Whitehead et al., 2016; Pöhlker et al., 2006).